Geophys. J. Int. (1995) **120,** 474–498

Determining surface-wave magnitudes from regional Nevada Test Site data

Bradley B. Woods and David G. Harkrider
Seismological Laboratory 252-21, *California Institute of Technology, Pasadena,* CA 91125, *USA*

Accepted 1994 July 21. Received 1994 July 21; in original form 1994 April 23

SUMMARY

We re-examine the use of surface-wave magnitudes to determine the yield of underground nuclear explosions and the associated magnitude-yield scaling relationship. We have calculated surface-wave magnitudes for 190 Nevada Test Site (NTS) shots using regional long-period seismograms from a combined super-network of 55 North American stations. Great effort went towards making the data set comprehensive and diverse in terms of yield, source location and shot medium in order to determine the portability of surface-wave magnitude scales. In particular, we examine Pahute Mesa, Rainier Mesa and Yucca Flat explosions detonated above and below the water table, and which range over three orders of magnitude in yield. By observation we find a low-yield measure threshold of approximately one kiloton (kt) for (assumedly) moderately well-coupled explosions recorded at near-regional (<500 km) stations, which have little microseismic noise. In order to utilize regional surface waves ($\Delta < 15°$) for quantifying sources and for discrimination purposes, we have developed related methods for determining time-domain surface-wave magnitudes and scalar moments from regional Rayleigh waves. Employing regional surface-wave data lowers the effective magnitude threshold. One technique employs synthetic seismograms to establish a relationship between the amplitude of the regional Airy phase, or Rayleigh pulse of the Rayleigh wavetrain and an associated surface-wave magnitude, based on conventional M_S determinations, calculated from synthetic seismograms propagated to 40°. The other method uses synthetic seismograms in a similar fashion, but the relationship used is a more straightforward one between scalar moment and peak Rayleigh wave amplitude. Path corrections are readily implemented to both methods. The inclusion of path corrections decreases the M_S variance by a factor of two and affects the absolute scaling relationship by up to a factor of 0.1 magnitude units. This latter effect is attributed to the particular station network used and the Green's functions used to obtain the 40° M_S values. Using a generic structure for the distance travelled past the actual source–receiver path minimizes the difference between magnitudes determined with and without path corrections. The method gives stable M_S values that correlate well with other magnitude scale values over a range of three orders of magnitude in source yield. Our M_S values scale very similarly to more standard teleseismic M_S values from other studies, although the absolute M_S values vary by ±0.5 magnitude units about ours. Such differences are due in part to the choice of M_S formula used. For purposes of future user comparisons, we give conversion values to the previous studies. Our most refined M_S values give the relationship $M_S = 1.00 \times \log_{10}(\text{yield}) + B$, where B is dependent upon source region and shot medium. This yield exponent of unity holds for events of all sizes and is in line with M_S-yield scaling relations found by other studies. When events are grouped with respect to source region, significantly better fits to these individual-site linear-regression curves are obtained compared to the fits obtained using a single, all-inclusive model. This observation implies that shot-site parameters and source structure can significantly affect

surface-wave-magnitude measurements. We present these M_S values primarily to augment the extensive historical analysis of explosion data based on surface-wave magnitudes by using regional data to increase the number of events with surface-wave magnitudes. These magnitudes are consistant with the teleseismically determined magnitudes of larger events. We present our preferred surface-wave moment values in a sequel paper.

Key words: North America, nuclear explosions, surface waves.

INTRODUCTION

We re-examine the use of surface waves for determining underground nuclear-explosion magnitudes, particularly for smaller yield, Y ($Y < 20$ kt), events. The surface-wave magnitude-yield scaling relationship for such low-yield events is not well defined. Even for larger yield explosions there is some debate as to the scaling relation between yield and the long-period energy radiation, as well as the relationship between M_S and m_b. Evernden & Filson (1971) found that $M_S = 1.4 + 1.3 \times \log(Y)$ for hard rock sites in North America, where log is understood to be $\log_{10}$. Marshall, Douglas & Hudson (1971) found that M_S scales with yield to the first power, with consolidated rock (tuff, salt, granite, andesite and sandstone) coupling 10 times more efficiently than detonations in alluvium. More recently Marshall, Springer & Rodean (1979) found that for events detonated in hard rock (salt or granite) or water-saturated material (below the water table) that $M_S = 2.16 + 0.97 \times \log(Y)$ and that $M_S = 1.88 + 1.06 \times \log(Y)$ for explosions above the water table. Taken together, these two populations yield the relationship $M_S = 2{\cdot}05 + \log(Y)$ (Bache 1982). Basham & Horner (1973) found the scaling relationship for explosions in consolidated rock at sites throughout the world (a majority of the events being from NTS) to be $M_S = 1{\cdot}56 + 1{\cdot}24 \times \log(Y)$. Sykes & Cifuentes (1984) found a worldwide empirical relationship of $M_S = 2.16 + 0.95 \times \log(Y)$ for explosions. Murphy (1977) found that the scaling law varied between events larger than 100 kt [$M_S = 1.2 + 1.33 \times \log(Y)$] and smaller events [$M_S = 2.14 + 0.84 \times \log(Y)$].

The above studies utilized data from a suite of sites to determine magnitude-yield relationships. Doing so is likely to add scatter to the results, for the shot medium, the source region, and regional propagation effects may all affect surface-wave amplitudes. We subgrouped our data set into specific source-region data subsets in order to ascertain whether or not the separated explosion populations have different magnitude-scaling relationships.

The data for this study are long-period vertical-component surface-wave records for 190 Nevada Test Site (NTS) events. The stations used are from several North American networks. Their respective instruments all have passbands that lie within the 6 to 60 s range. Surface waves are very useful for yield estimation purposes, for M_S is determined from relatively long-period seismic waves that are insensitive to high-frequency near-source effects, which may be caused by asymmetries in the shot cavity (Zhao & Harkrider 1991), spall (Taylor & Randall 1989; Day & McLaughlin 1991) or other possible mechanisms. These high-frequency source effects may cause appreciable bias in magnitudes that are based on higher frequency waves, such as the m_b and L_g scales. There are advantages to using body-wave measurements. Teleseismic body waves traverse mantle paths that are relatively homogeneous, whereas surface waves travel in crustal and upper-mantle waveguides that are known to have strong lateral inhomogeneities.

Evernden & Filson (1971) suggest, based on their observations of body-wave and surface-wave magnitudes of U.S. underground explosions detonated both within and outside of NTS, that the change in $M_S - m_b$ relationship from site to site is due to abnormal m_b values, rather than abnormal M_S values, and that regional-crustal and upper-mantle attenuation variations near the source (Δt^*) are responsible for the larger scatter in m_b-yield correlations. M_S measurements are also less sensitive to source-depth effects than are body-wave measured magnitudes (Marshall & Basham 1972). If it was not for contamination due to tectonic release, which has a more pronounced effect on long-period surface waves than body waves, and lateral inhomogeneity along the surface-wave propagation path near the surface of the earth, the long-period energy measured from surface waves might be a more stable measure of seismic yield than teleseismic body-wave measurements. It is the purpose of this paper to develop and apply a technique for reducing the contaminating effect of lateral propagation on M_S measurements.

Another advantage of using seismic moment or M_S is that empirical evidence and theoretical studies show that the scaling relationship between M_S (or log moment) and yield has an approximate slope of unity, i.e. $M_S = \log(\text{yield}) + B$, whereas the m_b-yield and $m_b(L_g)$-yield relationships have slopes between 0.65 and 0.90. As Evernden & Filson (1971) point out, a 0.3 error in m_b corresponds to a three-fold error in yield determination, while an equivalent error in M_S results in only a two-fold error in the yield estimate. Thus the error in yield estimation is inherently larger when obtained from higher-frequency magnitude measurements.

For lower-yield events it becomes necessary to include the data from regional stations ($\Delta < 25°$), for teleseismic surface-wave recordings have too low a signal-to-noise ratio (SNR), which makes them unusable. At regional distances surface waves are not well dispersed, having a prominent Airy phase pulse with a period between 6 and 20 s (Alewine 1972), so that it is not possible to measure M_S conventionally (that is measuring the amplitude of a stable, prominent 20 s surface wave). For North America in general, there is a minimum in the group velocity curve near 12 s for the fundamental Rayleigh wave (Marshall *et al.* 1979). To make accurate surface-wave magnitude measure-

ments, this energy bandwidth ought to be modelled as well as possible, for it is the predominant signal of the wavetrain.

To measure M_S we first model regional Rayleigh waves with theoretical seismograms. These synthetic wavefields are then propagated out to 40°, at which distance stable 20 s surface-wave magnitudes can be measured. In using this procedure several propagation-path models were tested to determine the effect of attenuation and seismic-velocity structure upon the M_S values. These calculated M_S values remain stable, have reasonably small errors and correlate well with associated m_b magnitudes and log yield for the event data set. The $M_S - m_b$ relationships are determined by a weighted least-square linear regression; both free- and fixed-slope curves were fitted to the data.

We also determine time-domain moment measurements from the same data. The moment is determined from the ratio of the maximum peak-to-peak amplitude of the surface wave train to that of a synthetic, with a given input-step moment, propagated to the same distance as the data. These two time-domain magnitude measurements (M_S and log M_0) give very consistent scaling results.

Besides comparing the M_S results with several different independent magnitude scales, the data have also been separated with respect to source region and shot material. No corrections were made in magnitude for shot-medium coupling effects, although such effects can be considerable, even for long-period energy (Werth & Herbst 1963), because such shot-site information would not necessarily be available for events detonated in other countries. This study is meant to test the effectiveness and portability of a surface-wave magnitude scale in the most general case.

We do not account for tectonic-release effects upon the magnitude measurements. Such effects are best accounted for with moment-tensor inversions of sources which involves more sophisticated data analysis. Standard M_S measurement techniques ignore this factor as well. The effects of tectonic release are considered in a sequel paper.

DATA

The data are long-period vertical seismograms recorded at North American stations for 190 explosions at NTS and consist of digitized World Wide Standard Seismographic Network (WWSSN) and Canadian Seismographic Network (CSN) records, Digital World Wide Seismographic Network (DWWSN), Lawrence Livermore Regional Seismic Network (LLNL) and Regional Seismic Test Network (RSTN) digital data. The analogue WWSSN and CSN data were digitized by ENSCO Inc. Fig. 1 shows a map of this 58 station super-network. Epicentral distances range from 220 km for NTS to GSC (Goldstone, California), to 4350 km for NTS to MBC (Mould Bay, Northwest Territories). For the smaller events, particularly Rainer Mesa explosions, only the nearer stations (distance < 1000 km) had usable data. Station coverage varies widely

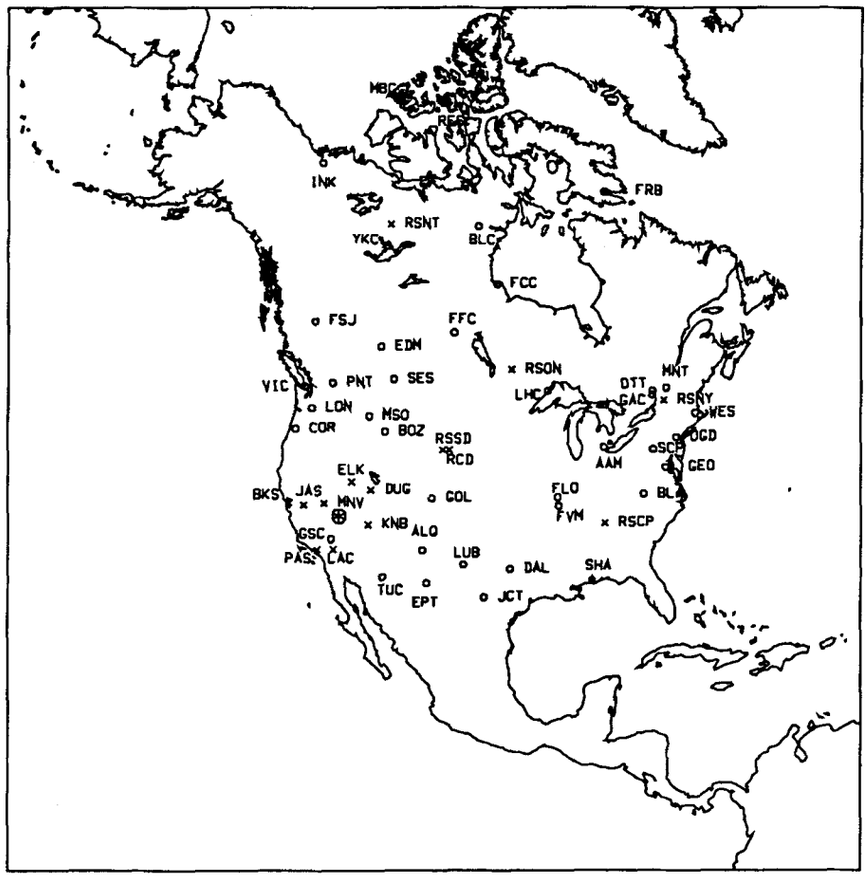

Figure 1. Map of the North American station network used in this study. The 'spoked wheel' is the Nevada Test Site.

between events. 22 of the smaller events (or very early events) only had one usable station seismogram each, while some events had over 30. The average number of stations reporting per event is approximately 10. For current and future geographical areas of monitoring interest it is reasonable to assume that only sparse networks will be able to record any given event, particularly smaller explosions (below 10 kt) or intentionally 'muffled' explosions, so it is important to see how well an explosion magnitude can be estimated with only a few observations.

Because our methods for determining magnitudes are done by means of time-domain measurements, analogue records can be readily used as well. We took advantage of this fact to add considerably more events (72 of the 190) to the sample population. These events were chosen with a mind to filling out the data set with respect to yield, depth to water table and geographic location.

We chose to confine our study to surface waves travelling solely along continental paths, i.e. within North America. Surface waves that propagate across oceanic-continental margins undergo significant modification in their waveforms because of the great lateral variation in crustal and upper-mantle structure at such boundaries. These propagation effects are not straightforward to model, and hence meaningful Green's functions, or transfer functions, are difficult to obtain. Without robust Green's functions it is hard to infer accurate source information from the data. Also, smaller events are not likely to be observed at the distant stations, which often include oceanic structure along their propagation path, and make these longer paths even less attractive to include in the monitoring network.

Of the 190 events, 48 are from Pahute Mesa, 30 are from Rainer Mesa, 105 are from Yucca Flat and seven others are from other sites in or around NTS, but outside of the three major test sites. Of these seven events, PILEDRIVER (detonated at Climax stock) was the only one for which digital data were available. For some specific stations, waveforms varied somewhat between events, depending upon source location. The PILEDRIVER data from a given station look appreciably different from those of any other events recorded at that same station. This was true for every station recording PILEDRIVER and probably is caused by differences in the source region for this explosion. PILEDRIVER was detonated in a granitic source region, north of the other sites. The source-to-receiver geometries for this event are approximately the same as those at the other NTS events, so the difference in waveforms appears to be a source effect rather than a propagation effect. Because PILEDRIVER was the only Climax Stock event with readily available data, no further examination of this site was carried out.

Figure 2 compares representative NTS vertical-component long-period data with synthetic Rayleigh waves for each source–receiver path. More than one event was used since no one event was observed at every station. The darker traces are the observations and the lighter trace below each

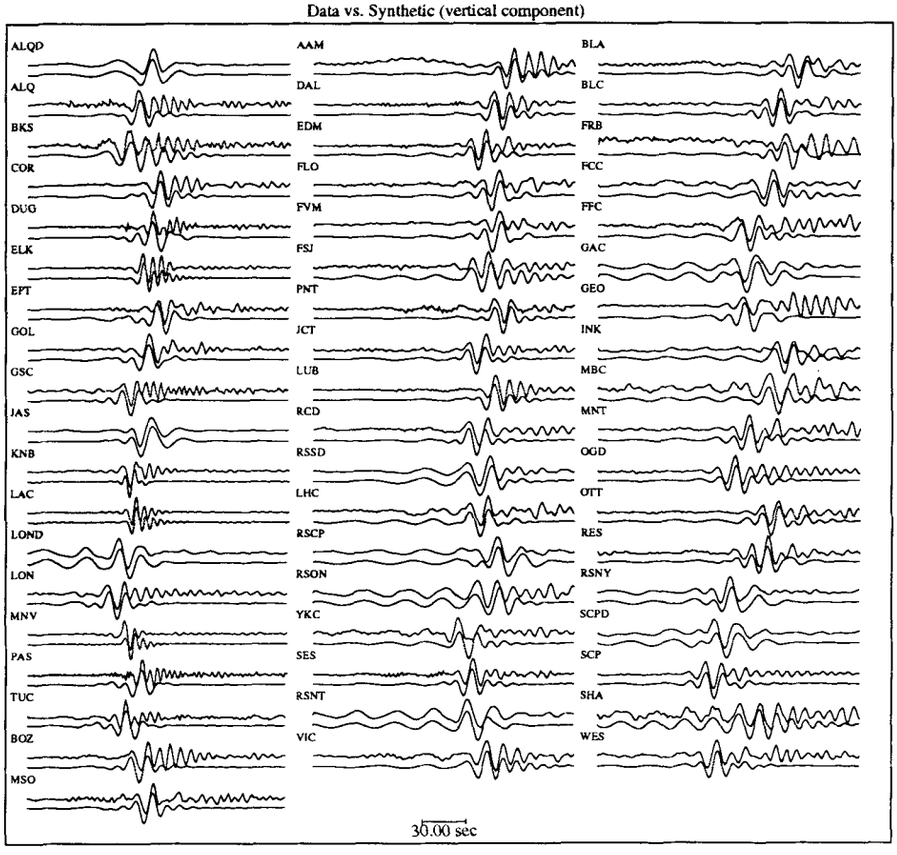

Figure 2. Comparison of vertical-component Rayleigh-wave waveforms. The data time series are the upper, thicker traces; the lower trace in each case is the fundamental-mode synthetic. All time series band-passed between 60 and 6 s.

is a synthetic seismogram made with the fundamental-mode Rayleigh wave only. The seismograms were bandpassed filtered between 6 and 60 s to suppress the long-period and short-period noise that would otherwise affect the peak-to-peak measurement of the Rayleigh pulse.

MAGNITUDE CALCULATION TECHNIQUE

We have developed a method to measure surface magnitudes indirectly. Because a large portion of the data for low-yield events is from stations recording at regional distances ($\Delta < 25°$), it is not possible to calculate M_S conventionally, for the Rayleigh wave is pulse-like, which precludes measuring a well-dispersed 20 s phase (Alewine 1972). We address this problem with the use of synthetic seismograms of the fundamental Rayleigh wave using an asymptotic relation for mixed-path surface waves.

For our mixed path expressions, we follow Levshin (1985) or Yanovskyaya (1989, page 44) and write the spectral Rayleigh wave vertical displacement for approximate propagation in a slowly varying laterally inhomogeneous media (e.g. Burridge & Veinberg 1977; Babich, Chikhachev & Yanovskyaya 1976; Woodhouse 1974; Yomogida 1985) as

$$w_0 = \frac{\exp(-i3\pi/4)}{\sqrt{8\pi\omega}} \frac{\exp\left[-i\omega\int_{P_0}^{P} ds/c\right]}{\sqrt{[J]_P}} \exp\left[-\int_{P_0}^{P}\gamma\, ds\right] \times \left[\frac{1}{\sqrt{UI}}\right]_P \left[\frac{W}{\sqrt{UIc}}\right]_{P_0} \quad (1)$$

where the energy integral is

$$I = \int_0^\infty \rho(z)[y_1^2(z) + y_3^2(z)]\, dz, \quad (2)$$

$\rho(z)$ is the local density distribution in the medium and we have used Saito's (1967) Rayleigh wave eigenfunction notation, $y_i(z)$. The eigenfunctions are normalized in such a way that the vertical-displacement eigenfunction, $y_1(z)$ is equal to 1 at the free surface, $z = 0$. This results in the horizontal displacement eigenfunction, $y_3(z)$, being equal to the Rayleigh mode surface ellipticity at this boundary. U and c are respectively the local group and phase velocities. By local we mean the eigenvalues and eigenfunctions that one would obtain for a laterally homogeneous half-space consisting of the vertical elastic and density distribution at that location. P is the receiver location and P_0 is the point-source location and quantities within the P or P_0 subscripted square brackets are evaluated at these locations. The integrals are taken along the phase-velocity-determined ray path between the two surface locations. J describes the geometrical spreading of the surface-wave energy. γ is the frequency-dependent attenuation coefficient due to the anelastic structure of the path, i.e. $\gamma = \omega/(2QU)$, where Q is the attenuation quality factor. The above expression is applicable in the absence of foci or shadow zones in the vicinity of the receiver. If there are foci along the path an additional phase factor of $\exp(i\pi/2)$ should be included for each foci. For an explosion, W is

$$W = M(\omega)\left[\frac{dy_1}{dz} - \frac{\omega}{c} y_3(z)\right], \quad (3)$$

where $M(\omega)$ is the isotropic or explosion spectral seismic moment. We also assume a step for our explosion history, i.e. $M(\omega) = M_0/(i\omega)$.

Since we will assume that the directions of the horizontal gradients of the material properties are approximately aligned in the direction of the source to receiver, the ray path is a straight line and $J = r$, which is the distance between the two locations. We further assume that the lateral inhomogeneity can be considered to be made up of n homogeneous segments of radius r_i, i.e. $\Sigma r_j = r$. For comparison with Stevens (1986), who used a similar expression to estimate seismic moments for explosions, and earlier works on which his expressions were based (e.g. Bache, Rodi & Harkrider 1978; Harkrider 1981), we write W in terms of K where

$$K = y_3(z) - \frac{c}{2\mu\omega} y_2(z) \quad (4)$$

and y_2 is the normalized vertical normal stress eigenfunction. The relation between K and W is obtained by substituting

$$\frac{dy_1}{dz} = \frac{1}{(\lambda + 2\mu)}\left[y_2(z) + \frac{\omega}{c}\lambda y_3(z)\right] \quad (5)$$

into the previous W expression.

Now we can write the multipath displacement as

$$w_0 = -\frac{\exp(-i3\pi/4)}{\sqrt{2\pi\omega}} \frac{\beta_1^2}{\alpha_1^2} \frac{M_0}{c_1} \frac{\exp[-i\omega(r_j/c_j)]}{\sqrt{r}} \times \exp(-\gamma_j r_j)\left[\frac{1}{\sqrt{UI}}\right]_n \left[\frac{K}{\sqrt{UIc}}\right]_1 \quad (6)$$

where the summation convention of repeated subscripts is used. The subscript '1' denotes the local quantities for the source medium and the subscript 'n' the local quantities at the receiver. The shear velocity is denoted by β and the compressional velocity by α. For a given moment, M_0, the ratio of the square of these two quantities plays a key role in determining the amplitude effect of various shot media. To this order of approximation the spectral amplitude neglecting attenuation is only dependent on the local properties at the source and receiver. The attenuation and phase are dependent on the local properties along the whole path.

With the substitution

$$A = \frac{1}{2cUI} \quad (7)$$

(Harkrider & Anderson 1966; Harkrider 1981) and multiplying by $-\sqrt{c_n/c_1}$, we obtain the same expression as used by Stevens (1986) to obtain his path corrections from NTS to 24 WWSSN station in United States and Canada and to 12 SRO stations. For his models $n = 2$. The negative sign results from the differences in our sign criteria for vertical displacement. In Stevens (1986) vertical displacement is positive up while in this article it is positive down. The phase-velocity factor is due to the use of wavenumber spreading by Bache *et al.* (1978), Harkrider (1981), and Stevens (1986) compared to geometric spreading by the others. Bache *et al.* (1978) based their expressions on the conservation of lateral-energy flux while these expressions are from the main term in an asymptotic expansion.

Glover & Harkrider (1986) performed numerical tests in order to estimate the frequency range for which these approximations were valid for Rayleigh waves generated at NTS where the source region may be limited by sharp boundaries such as in the low-velocity basin at Yucca Flat. Rayleigh wave seismograms were calculated for explosive sources at depth in a finite vertical cylinder with contrasting elastic properties representative of the various test areas at NTS embedded in a vertically stratified propagation media. The technique couples laterally inhomogeneous finite-element calculations of the source region with Green's functions for teleseismic Rayleigh waves using the elastodynamic representation theorem. The details of the technique can be found in Harkrider (1981) and Bache, Day & Swanger (1982). The spectra for these Rayleigh waves were then compared with those, which used the two approximations to cross the sharp boundary. It is surprising that both approximations worked as well as they did since they are based on a gradual transition. It was found that both approximations worked equally well for periods greater than four seconds, and that for shorter periods the asymptotic approximation used in this paper is better. The period range is dependent on the material contrast and the vertical extent of the contrast but this mixed path approximation is certainly adequate for the determination of long-period moments and surface-wave magnitudes from NTS Rayleigh wave observations at continental stations.

It is interesting to note that for this geometry, i.e. $n = 2$, the Rayleigh wave transmission coefficient, $T(\omega)$, of Bache *et al.* (1978)

$$T(\omega) = \left(\frac{c_2 A_2}{c_1 A_1}\right)^{1/2} = \left(\frac{U_1 I_1}{U_2 I_2}\right)^{1/2} \tag{8}$$

is identical to the factor R of Levshin (1985) and was used in both articles to illustrate the effect of mixed paths on the amplitude of Rayleigh waves.

For each source-to-receiver path, a theoretical Rayleigh wave is generated. The earth model used to create this synthetic is meant to reflect the average earth structure between NTS and the given station. The earth models used in this study were determined from inversions of dispersion and attenuation data as well as forward modelling of the waveform to fine tune the models. The criteria for determining the goodness of fit of the synthetic to the data are dispersion, absolute traveltime and waveform fit (relative amplitude of different dispersed phases). Hence the synthetic seismogram displays the same spectral and time-domain waveform characteristic as the data which it simulates (see Fig. 2). This was done for all paths. The paths to WWSSN and Canadian stations were taken from the explosion moment study by Stevens (1986). We determined the RSTN, LLNL and DWWSN path structures.

To determine M_S for a particular source–receiver geometry two synthetics are generated. One, which is propagated the actual path distance, that is meant to simulate the data and one which is propagated to 40°. At 40° the surface wave train is well dispersed and stable, so that a conventional M_S value can be calculated. Fig. 3 illustrates this method. The upper set of seismograms are a comparison of data to its corresponding synthetic seismogram. For this particular example the station COR (Corvallis, Oregon) and the event LOWBALL are used. The data is the solid line and the dashed line is the synthetic time series. Note that the waveform fit (dispersion and relative amplitude) is exceptional. This feature is important in order to make maximum peak-to-peak amplitude comparisons. The middle figure schematically shows the propagation paths for the synthetic seismograms. The path of length R is the actual source-to-receiver distance. The longer path is of length 40°. The bottom figures are of the two synthetic seismograms. The left one is calculated for the distance R (10.4° in this case) and the right seismogram is the one propagated out to 40°. They are plotted to the same time-scale. Note the much better dispersed wave train in the 40° case. The arrows in the right-hand figure mark the cycle or phase of the record which is used to obtain a M_S value.

To calculate M_S we use a modified version of the von Seggern formula (von Seggern 1977):

$$M_S = \log(A/T) + 1.08 \times \log(\Delta) + 4.38, \tag{9}$$

where A is one-half the maximum peak-to-peak amplitude (in microns) for periods between 17 and 23 s of a well-dispersed wave train measured from the vertical record, T is the period of the arrival measured in seconds, and Δ is the propagation distance in degrees. The original formula was modified to include the period correction and is the same at a period of 20 s. This formula was chosen because the distance coefficient (1.08) more closely approximates the effect of attenuation along continental paths (Basham 1971; Marshall & Basham 1972). Evernden (1971) found the distance coefficient to be 0.92 for M_S measurements at less than 25° and 1.66 for measurements at greater distances. This latter attenuation coefficient is more characteistic of mixed continental-oceanic path 20 s surface waves. Basham (1971) also found that the surface-wave magnitude distance coefficient for regional Rayleigh waves ($10 < T < 14$ s) is between 0.7 and 0.8. Marshall & Basham (1972) make similar assertions, but employ a distance correction which is a function of distance as well.

A vertical-component measurement has two advantages over horizontal-component measurements. The horizontal components usually have lower signal-to-noise ratios than the vertical component and generally are more likely to be contaminated by Love wave signals which may be generated by tectonic release, source effects, or scattering due to lateral variations in the earth's structure.

Both the regional and teleseismic (40°) synthetics are generated with the same site and source function, so that the peak-to-peak amplitude of the Rayleigh pulse of the regional synthetic can be directly related to the M_S value determined for a theoretical Rayleigh wave train propagated out to 40°. In order to reduce the effect of the various network instruments on the M_S measurement and any path correction, which might be made, the magnitude measurement was made on synthetics generated with the same long-period WWSSN instrument while the amplitude of the synthetic Rayleigh pulse was generated using the actual station instrument response. The relationship between the data peak-to-peak amplitude and its indirectly determined M_S is:

$$M_S(\text{data}) = M_S(\text{synth}\,|_{40^\circ}) + \log\left[(PPA\,|_{\text{data}})/(PPA\,|_{\text{synth}})\right], \tag{10}$$

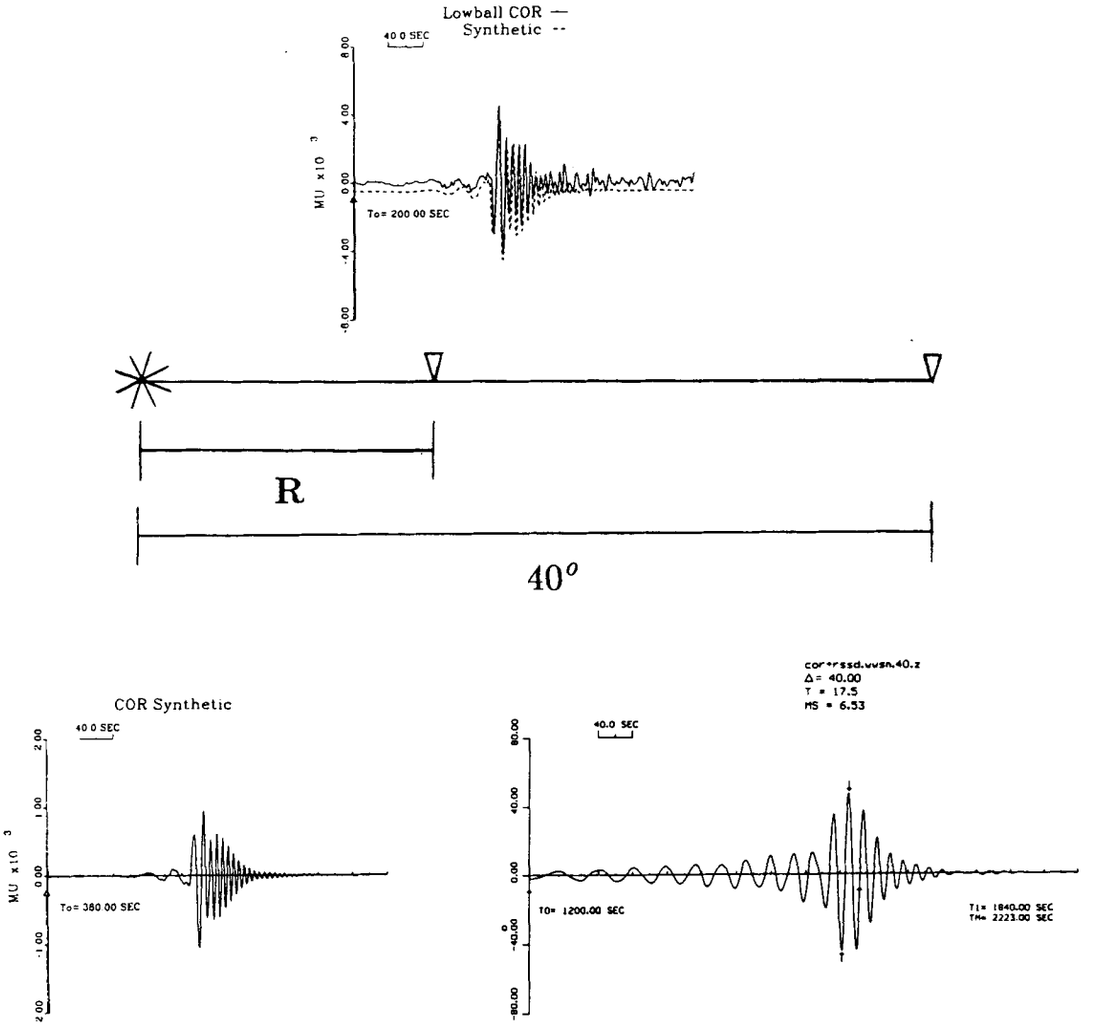

Figure 3. Schematic of the M_S calculation method: (a) the top figure is a comparison of observed-to-synthetic seismograms for the event Lowball recorded at the WWSN station COR ($\Delta = 10.4°$). This record shows a prominent Airy phase with a dominant period that is considerably less than 20 s. The solid line is the observed time series, and the dashed line is that of the synthetic seismogram. Both time series have been bandpass filtered between 60 and 6 s. (b) The middle figure shows the paths for which synthetic Rayleigh waves are calculated. There are two receiver distances. One, R, is the distance between the actual receiver and the source. The other distance is 40°. A synthetic generated for the distance R is made with a structure that best models the regional seismogram. (c) The bottom two figures show synthetic seismograms calculated for the two receiver distances for the COR path model. The left-hand one is for the actual regional path distance R; it is flipped in polarity with respect to the same synthetic in the top figure. The right-hand one is a Rayleigh wave propagated to 40°; the arrows denote the pulse that is used to calculate M_S. Notice that the dominant period for this case is 17.5 s. This pulse is considerably closer in period to 20 s than that of the regional seismogram which has a period near 12 s.

where PPA is the peak-to-peak amplitude of the Rayleigh pulse. A path correction may be included in this expression. This path correction is the difference between the individual path synthetic-derived M_S and the average theoretical M_S for the entire network. It also differs from a classical station correction that comes from the data and not the synthetics. Secondary station corrections based on the data were not used in this paper. For each source–receiver pair, a M_S is calculated from a synthetic seismogram propagated to 40°. Each such synthetic has the same site and source size, so ideally one would want all M_S values so measured to be equal in value. Yet this is not so, for each path's dispersion and effective attention at the periods measured may be different. The difference between the mean network synthetic M_S and a particular receiver M_S is the path correction. A negative path-correction value implies that the theoretical 40° station M_S is larger than the network average. Table 1 lists the network path corrections used.

The question arises whether or not it is valid to use the average earth structure for a particular path to propagate a surface wave to 40° when the earth model is only meant to reflect the seismic properties of the earth for a path that may only be a small fraction of this distance. This is particularly true of the shortest paths for which the seismic waves traverse only western North America, an area of relatively high attenuation compared to the continental craton and shield areas. A surface wave propagated 40° along a characteristic tectonic North American crust and mantle

Table 1. Network path corrections.

Dominant Period	Path Correction Dispersion	Path Correction Single Path	Path Correction Mixed Path 1	Path Correction Mixed Path 2	Station Name
11.5	-0.64	0.20	-0.07	-0.11	AAM
12.0	-0.61	0.18	-0.02	0.17	ALQ
13.5	-0.50	0.57	0.08	0.27	BKS
15.0	-0.38	-0.24	-0.28	-0.32	BLA
10.5	-0.71	0.18	0.00	-0.47	BLC
11.0	-0.67	-0.26	-0.02	0.16	BOZ
11.5	-0.64	-0.12	0.07	0.14	COR
11.0	-0.67	0.35	-0.12	0.09	DAL
12.0	-0.61	-0.03	-0.02	0.19	DUG
11.0	-0.67	-0.26	0.10	0.03	EDM
11.2	-0.66	0.26	-0.03	0.20	ELK
12.0	-0.61	-0.03	-0.03	0.12	EPT
12.0	-0.61	-0.22	0.06	0.01	FCC
12.5	-0.57	-0.22	-0.02	0.01	FFC
12.0	-0.61	-0.24	-0.12	-0.09	FLO
11.5	-0.64	0.18	0.18	-0.02	FRB
13.5	-0.50	0.45	0.20	0.25	FSJ
11.5	-0.64	-0.24	-0.12	-0.09	FVM
16.0	-0.30	0.18	0.40	-0.29	GAC
15.0	-0.38	-0.24	-0.15	-0.47	GEO
11.5	-0.64	-0.11	0.03	0.08	GOL
11.0	-0.67	0.26	-0.04	0.22	GSC
12.0	-0.61	-0.40	-0.11	-0.23	INK
11.0	-0.67	0.18	0.04	0.13	JCT
11.2	-0.66	1.06	0.02	0.26	KNB
11.2	-0.66	0.26	-0.05	0.20	LAC
12.5	-0.57	-0.13	-0.01	0.00	LHC
11.0	-0.67	0.20	0.01	0.17	LON
11.5	-0.64	-0.19	0.06	0.03	LUB
12.5	-0.57	-0.44	0.26	0.06	MBC
11.5	-0.64	0.18	0.37	-0.39	MNT
11.5	-0.64	0.26	-0.04	0.22	MNV
11.0	-0.67	-0.26	-0.03	0.14	MSO
10.5	-0.71	0.16	0.30	0.19	OGD
11.5	-0.64	0.18	0.40	-0.28	OTT
12.5	-0.57	1.12	0.03	0.27	PAS
11.0	-0.67	-0.26	-0.03	0.11	PNT
11.0	-0.67	-0.26	-0.04	0.10	RCD
11.5	-0.64	-0.39	-0.39	-0.59	RES
11.0	-0.67	-0.53	-0.17	-0.31	SCP
11.0	-0.67	-0.26	-0.05	0.07	SES
12.5	-0.57	0.03	0.04	0.09	SHA
11.5	-0.64	-0.03	-0.04	0.15	TUC
11.5	-0.64	0.45	0.16	0.27	VIC
11.5	-0.64	0.22	-0.30	-0.41	WES
12.5	-0.57	-0.40	-0.20	-0.23	YKC
19.5	-0.04	0.18	-0.02	0.17	ALQD
16.5	-0.27	0.20	0.01	0.17	LOND
16.5	-0.27	-0.53	-0.17	-0.31	SCPD
15.0	-0.38	-0.51	0.02	0.02	RSCP
16.0	-0.30	-0.09	-0.05	0.09	RSSD
15.5	-0.34	-0.19	-0.07	-0.05	RSON
16.0	-0.30	0.18	0.33	0.22	RSNY
15.5	-0.34	-0.40	-0.20	-0.23	RSNT
18.0	-0.16	1.21	0.01	0.19	JAS

model (NTS to DUG, for example) for 40° will be much more attenuated than a wave propagated the same distance through an average structure from NTS to eastern North America (NTS to SCP, for example). Hence the calculated M_S for the NTS to DUG structure would be smaller than the NTS to SCP M_S.

There are several methods to correct for this path-dependent effect. As explained above one may implement path corrections that account for the theoretical difference in attenuation between paths. Another means is to make a mixed-path structure that has the appropriate path structure from the source to the actual station distance, with the rest of the path out to 40° being a generic seismic velocity and attenuation model. For the cases in this study where the structures that comprise the mixed path are both continental structures (i.e. not too dissimilar) the approximation is robust enough for the synthetic-seismogram calculations.

We have implemented both procedures individually and in conjunction to see what their effects are. Another method would be to include empirical station corrections (Yacoub 1983; Given & Mellman 1986). Path correction effects are discussed in the results section.

Besides the M_S determination, we also calculated a time-domain moment for the same data. This time-domain, scalar moment is determined as follows:

$$M_0(\text{data}) = M_0(\text{synth}) \times [(PPA\,|_{\text{data}})/(PPA\,|_{\text{synth}})], \qquad (11)$$

where PPA is the peak-to-peak amplitude of the Rayleigh pulse or Airy phase. This method is simpler than the M_S method and has the added advantage that the synthetic involves only two structures: the source region and the propagation path to the station. Path corrections were not incorporated into the time-domain M_0 determinations since the propagation-path synthetic takes the place of a path correction and we are not correcting to a generic (RSSD) structure. Making a correction based on the difference between the average station value and some mean for a collection of events is a form of the classical empirical station correction and is most useful when there are only a few stations reporting since a zero sum of the corrections is the usual constraint (Given & Mellman 1986). The mean moment can then be converted to an M_S using the moment-M_S relation for the generic structure (RSSD) propagated to 40°, i.e. the theoretical RSSD station magnitude

$$M_S(PPA) = \log M_0(PPA) - 11.38. \qquad (12)$$

Figure 4 plots M_S versus $M_0(PPA)$ for the entire data set. The correlation between the two types of magnitude measurements is extremely good. The regression constant 11.43 is very close to the theoretical value 11.38 given above. Thus the difference between our best mixed-path M_S regression with moment, and the M_S moment relation for a pure path of the generic RSSD model is only 0.05 magnitude units. On first glance it might appear that both techniques are identical. However, even if all the stations had the same moment, the individual station magnitudes would be different due to different extended path lengths and possibly different structures from the station out to 40°. We try to reduce this difference by making the additional correction to a mean of the theoretical values for all stations

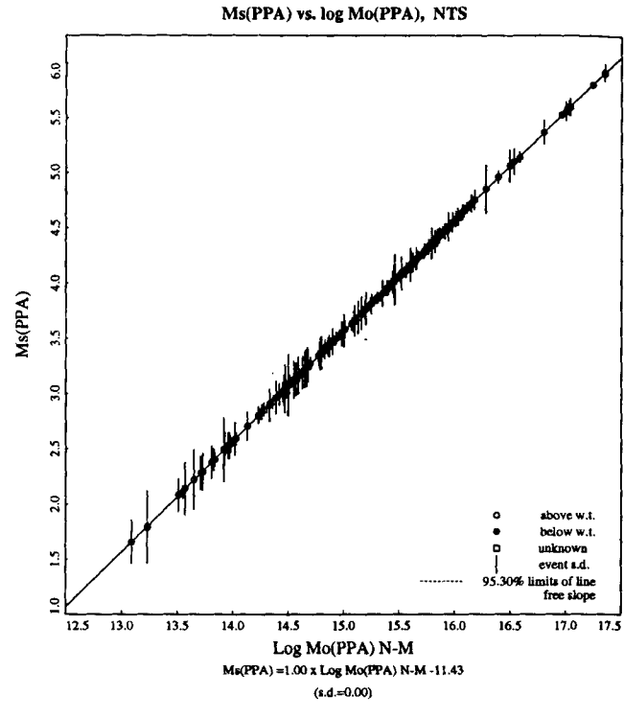

Figure 4. Time-domain M_S values regressed versus time-domain moments for all the events in this study. Note the extremely good correlation between the two scales. Vertical error bars are the variance for the individual events.

in the mixed-path evaluation. These observations imply that the RSSD model is a good average model for the network and that our M_S calculations are sound and result in robust measurements of surface-wave magnitude, which are not too dependent on which of the two techniques we use. In our analysis of the data we will use only M_S measurements. A table of the $\log M_0$ and their standard deviations will be given in Woods & Harkrider (1995).

Source structure significantly affects absolute surface-wave amplitudes, and hence surface-wave magnitudes or moments. For all of the synthetic seismograms generated, we used the Stevens (1986) and Given & Mellman (1986) NTS-source elastic structure, which is basically a Pahute Mesa velocity structure. By numerical simulations using a variety of different NTS structures, we found that for the frequencies of interest and sources in the upper 6 km the primary effect was due to the difference in shot-point velocity ratios. The size of the effect can be predicted extremely well from their explicit presence in the mixed-path expression, eq. (6). As an example, our Green's functions are computed for an explosive source at a depth of 600 m. In the Stevens (1986) source structure, the second layer starts at a depth of 500 m. There is a significant difference between the Poisson's ratio of the surface and second layer in the source earth structure. The log difference between the square of their compressional to shear velocities would predict from eq. (6) an M_S difference of 0.17. The actual difference between the M_S of a surface explosion and our Green's function is 0.16 with the near-surface explosion smaller as predicted. In order to reduce the effect of differing shot-point velocity ratios, Stevens (1986) suggested a new explosion moment, M_0',

defined by

$$M_0' = 3\frac{\beta^2}{\alpha^2} M_0. \quad (13)$$

For a shot-point medium with Poisson's ratio of 0.25 ($\alpha^2/\beta^2 = 3$) the value of the moment is unchanged.

In Fig. 2, we see that for the WWSSN stations, denoted by three letters, the period of the dominant phase is significantly lower than the recommended lower cut-off of 17 s for the standard M_S formula. This period was determined by taking twice the time difference between the arrival of the largest peak and trough. We also calculated the 'instantaneous period' of this arrival and found it to be essentially the same value. The dominant period at each station is given in Table 1. For the WWSSN stations, the periods are between 10 and 15 s. Most are near 11 s. For the digital stations, denoted by four letters, the dominant period is between 15 and 19.5 s, with the average being 16.5 s. An alternative approach for using the maximum amplitude of Rayleigh wave observations where the dominant period is significantly different from 20 s was developed by Marshall & Basham (1972). Using the stationary-phase approximation they determined a path correction, which corrected for the dispersive characteristics of the path. Using observed dispersion curves for North America, Eurasia, mixed ocean-continent, and pure ocean paths, they were able to determine an M_S correction based on the period of an observed Airy phase to the 20 s period arrival in North America or Eurasia. The North American dispersion correction appropriate for the dominant period measured at each station in our network is also given in Table 1 (column 2). An advantage of our technique is that our path corrections are independent of recording instrument whereas Marshall & Basham's correction depends on the dominant period, which depends not only on dispersion but also instrument response. As an example, the station ALQ has a dominant period of 12 s and ALQD has a dominant period of 19.5 s.

An advantage that time-domain estimates of M_S or M_0 have over spectral estimates can be seen in Fig. 2. Except for the work of Patton (e.g. Patton 1991), the Green's functions used for spectral estimates of explosions have been fundamental Rayleigh and Love waves. As can be seen from the figure, it is very important to isolate the fundamental surface wave in the data for taking its spectra for moment estimates. The Rayleigh waves at almost every station show the additional presence of higher modes. The higher modes are primarily due to constructive interference of multiple reflected shear waves and are therefore very sensitive to lateral variations in crust and upper-mantle structure. This is especially true for non-parallel layers with sharp contrasts. Therefore, in the presence of nearby signals or noise, it makes more sense to use the larger time-domain amplitudes of the fundamental-mode Airy phases at regional distances. Because of the possibility of tectonic release, it is also necessary to determine the polarity of the surface wave. Again this is best done in the time domain, especially for Love waves.

If a spectral estimate is desired, comparing the Green's function with the data in the time domain should allow one to determine time windows and tapers so as reduce the contamination of spectral-amplitude estimates with higher modes and spurious scattered arrivals at intermediate ranges. And at close ranges where this may not be possible, it should help in deciding which time-domain amplitude measurements best represent the spectral amplitudes of the fundamental modes.

The question remains how well do either of these two measurements compare to spectral-moment estimates. For the events for which digital data were available, spectral-domain moments were also determined. Spectral moments were calculated using the method of Stevens (1986), with the exception that station corrections were not included in our moment calculations. Spectral moments were calculated in the bandwidth between 6 and 60 s. These spectral moments will be referred to as M_0. Moments were also obtained by inverting for an isotropic (explosion source) component (M_I) and a deviatoric component (caused by tectonic release or an asymmetric source cavity) of moment ($M_\#$). Details of these moments are the subject of a later paper by the authors (Woods & Harkrider, in preparation).

We compare the time-domain moments with these two types of spectral-domain moments. Fig. 5(a) compares $M_0(PPA)$ to $M_0(\omega)$ and Fig. 5(b) compares $M_0(PPA)$ to $M_I(\omega)$. $M_0(\omega)$ refers to the average spectral scalar moment and $M_I(\omega)$ refers to the isotropic source component determined from a moment-tensor inversion scheme (Woods & Harkrider, in preparation). $M_0(PPA)$ correlates well with the two types of spectral moments. The advantage of time-domain moments is that analogue data can be used directly and the effective SRN is lower than for spectral-moments methods, thus smaller events can be measured.

In the top figure there is some scatter in the moment correlation for several of the smaller events, with the time-domain moments being significantly larger than the spectral-domain moments. Most of these outlying events are Rainier shots, none is from Yucca and only one, REX, is from Pahute. REX ($M_0(PPA) = 15.35$, $M_0(\omega) = 14.87$) was detonated below the water table and had an anomalously large deviatoric moment component (Woods & Harkrider, in preparation). Since many more stations were used in the determination of the time-domain moments with a more complete azimuthal coverage, one would expect them to be less affected by the deviatoric component, which at NTS is speculated to be such that it will average out with adequate azimuthal coverage. The scatter is somewhat less in the $M_0(PPA)$:$M_I(\omega)$ curve (Fig. 5b). In particular, REX no longer stands out, although several of the Rainer events lie well off the scaling curve. These outlying Rainier events can be explained in several ways. First, these events are relatively small and are only measured at very few stations (sometimes only one to three stations), thus the scatter, or error, in the moment measurement is larger. Also the spectral moment is more susceptible to noise contamination since it requires the isolation of a segment of the surface wave train from noise and the time-domain measurement only requires that the maximum amplitude not be too distorted by noise. One problem with this explanation is that there are other small events recorded at Pahute Mesa and Yucca Flat that lie right on the moment scaling curve (Fig. 5a) and these events are no better recorded than the Rainier events. Another possibility is that these outlying events

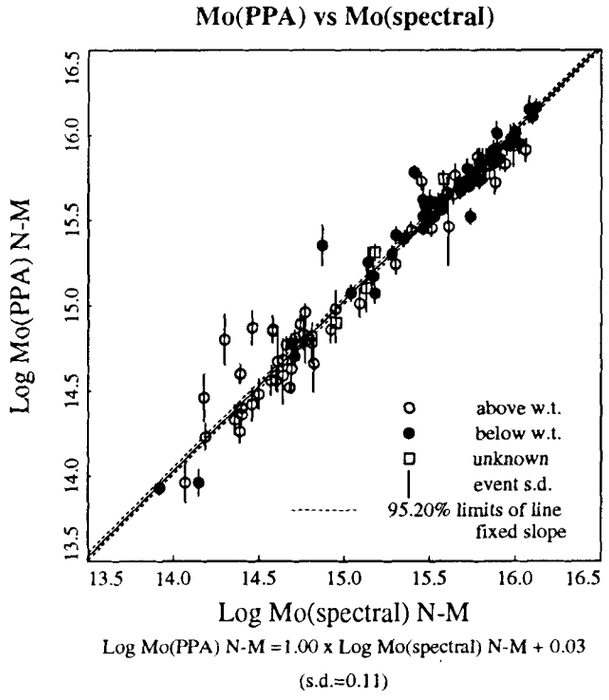

Figure 5. Time-domain log moments regressed against spectral-domain log moments. In the top figure spectral moments were determined assuming an isotropic source only, while in the bottom figure the spectral moments were determined by inverting for a isotropic source + a double-couple source. The regressions were constrained to a slope of unity.

reflect differences in source spectra. As discussed previously, the time-domain moments measure energy predominantly in the 10–14 s range, the period range of the continental Airy phase, whereas the spectral moment is an average of the spectral ratio between 6 and 60 s. So, it is possible that the Rainier test sites excite more high-frequency energy than do either the Phaute or Yucca site. This effect was seen in data at several of the closer stations, in particular.

DATA ANALYSIS AND RESULTS

The seismograms were bandpassed filtered between 6 and 60 s to minimize contaminating noise as described previously. The vertical records were visually inspected to ensure that the correct time window was used and that their signal-to-noise ratio was about 2.0 (approximately). M_S values were then calculated for the data as per the method described above (eq. 9) with several variations. The synthetic seismograms were also bandpassed filtered between 6 and 60 s for consistency. The M_S values are plotted against seismic magnitudes of several scales for the same set of events. It should be noted that no complete magnitude list was available for all 190 events.

We chose to compare or plot our data primarily with body-wave magnitudes determined by Lilwall & McNeary (1985). The Lilwall–McNeary (LM) data set contains 143 of the 190 events examined by us and is believed to be a well-determined and self-consistent list of m_b values that have small errors due to, among other things, the inclusion of network station corrections. Fig. 6 shows the m_b–yield relationship for events in this study for which m_b and yield information were available. It is important to notice that events above and below the water table separate into two distinct populations. For this data set this separation is only apparent near the cluster of events with m_b's around 5.4.

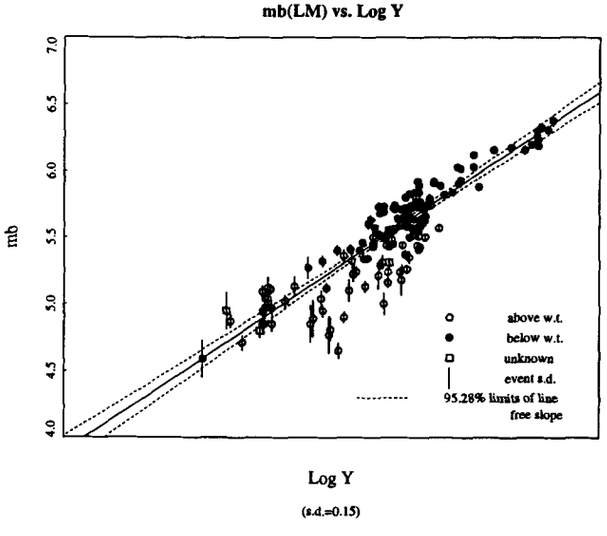

Figure 6. Lilwall m_b versus log Yield for events from this study. The solid line is the best-fitting regression line. The dashed lines show the 95 per cent confidence interval of this line. Lines through the data points represent one standard deviation in a datum measurement. Blackened circles represent sources beneath the water table, open circles are events above the water table and open squares are events for which this information is not known. Events detonated below the water table have a larger m_b for a given yield. Besides this separation of data, there is little scatter to the data. The consistency of the m_b–yield relationship makes it reasonable to use these m_b values to plot our M_S measurements against.

Also notice the very small error bars for this data; for many events the error bars are smaller than the symbols demarking a data point. The solid line is the best-fitting, least-squares curve, with the dashed curves being the two-sigma confidence interval of the regression relationship. The correlation between m_b and yield is good, with the scatter mostly being due to the above-water table shots. The slope of the regression curve is 0.67.

This scaling curve slope is slightly lower than that found in other studies of teleseismic m_b–yield scaling relationships. Marshall *et al.* (1979) found that m_b was proportional to $Y^{0.74}$ for well-coupled Yucca flat explosions, and proportional to $Y^{0.78}$ for explosions throughout NTS and Amchitka. Longer period telesiesmic body-wave magnitudes m_{LPP} introduced by Basham & Horner (1973) show that for events in tuff and rhyolite the amplitude of the arrivals is proportional to $Y^{0.72}$. Murphy (1977) compared theoretical m_b–yield scaling relations for cube-root scaling models and the modified Mueller & Murphy (1971) source model. He found that the yield exponent varies between 0.6 and 1.0 for the cube-root model in the yield range of interest, whereas the exponent is a constant 0.85 for their modified source model. Schlittenhardt (1988) found m_b to be proportional to $Y^{0.82}$ for NTS explosions. The empirically derived curves have errors in their slopes of the order of 0.05 to 0.1 units and are based on small sampling populations. The LM m_b–yield scaling relationship is determined from a significantly larger data set, making it at least as reliable as any other empirical scaling curve.

The same scaling law slope (~0.67) holds for the LM data when they were separated with respect to test-site and shot-medium coupling (whether detonated above or below the water table). There is consensus in the literature that that seismic coupling is a function of the percentage dry (or gaseous) porosity of a material. In a study of small-scale, high-explosive experiments with 15 rock types, Larson (1981) found for a given size explosion that the elastic radius of a porous material (such as tuff) increased with increasing water content. The dominant non-linear mechanism (within the plastic radius) working at low yields appears to be pore crushing of the surrounding material (Stevens 1991). Non-linear finite-difference calculations (Bache 1982) also indicate that porosity is the most important characteristic of NTS tuff for seismic-coupling purposes. In the same study, source functions for Yucca Flat wet and dry tuff are significantly different, with the long-period amplitude of wet tuff being larger by 50 per cent and its corner frequency being lower. Springer (1966) has observed this effect for teleseismic *P*-wave amplitudes. Patton (1988), Gupta *et al.* (1989), and Vergino & Mensing (1989) have observed this coupling effect in regional phases such as L_g, P_n and P_g.

Several sets of synthetic Rayleigh waves were generated at the 40° distance for calculating M_s. One set was propagated along the single-structure model (hereafter referred to as the single-path case) which reflects the average earth structure between NTS and a given station. We also generated mixed-path synthetics for which that part of the path beyond the actual source–receiver distance, out to 40°, the surface wave is propagated along a generic earth structure. The NTS–RSSD Earth structure was chosen for this generic path section, as it is a relatively simple structure that generates stable surface waves and it is roughly an intermediate range station (distance < 1900 km), so that its structure can be considered to be an 'average' North American structure for the network.

Surface magnitudes were first calculated from the 40° synthetics generated with a single-structure propagation path. Figs 7(a) and (b) display single-path m_S values, calculated as described above, versus body-wave magnitude (m_b). These m_b's are those of Lilwall & McNeary (1985). In the upper figure (7a) M_S is calculated without path corrections, whereas M_S is calculated with path corrections in the lower figure. The vertical error bars represent the one standard-deviation confidence interval for each M_S value. The solid line is the best-fitting weighted least-squares regression of the data, with the weighting factor being inversely proportional to individual event variances. The dashed lines represent the two standard-deviation error (assuming a Student *t* distribution) of the fit of the line to the data. Since Student *t* statistics (Lapin 1983) are functions of the sample size, the confidence level will vary with data set size. Solid black circles are shots below the water table, open circles are shots above the water table, and open squares are shots for which this information is not known. Note the error bars are approximtely 50 per cent larger for the uncorrected M_S's (Fig. 7a) than for the case of path-corrected M_S's (Fig. 7b). The scatter in the data is also significantly less for the path-corrected M_S's as evidenced by the reduction of the standard deviation of the free-slope regression. Although, it should be noted here and for the following discussion that the success of these techniques is not in how well they reduce the standard deviation from some assumed linear relation between surface and body-wave magnitudes, but how well they reduce the variance or standard deviation of the magnitude determination of an individual event, and even more important, their ability to include small events in the data base where teleseimic data was too sparse for determining a classical M_S. On the other hand, it is interesting that the standard deviation for the LM body-wave magnitudes versus yield is 0.15 and our best regression between M_S and their m_b for the same explosion data set is 0.26. Both regressions are improved when the events are separated into different populations. When we get to Figs 15 and 16, which are our regressions on log yield, you will see that our regression standard deviations are quite competitive with those of m_b for events restricted to NTS below the water table and Rainier.

There are two significant effects of including path corrections. One is the reduction in variance of individual magnitudes. Without path corrections the individual station magnitudes have a bi-modal distribution reflecting the two generic earth models of North America: the tectonic western and stable cratonic eastern crust and upper-mantle structures. The path corrections bring in the outlying station magnitude values towards the mean value. Including path corrections for the single-path derived M_S's increases the average value by 0.14 units (or 32 per cent). This effect can be attributed to the smaller events that are brought more in line with the curve containing larger events. This in turn is due to the fact that the smaller events are only observed at nearer stations in tectonic North America (TNA), for which path structures exhibit higher attenuation than do more cratonic or shield-like models, so that surface

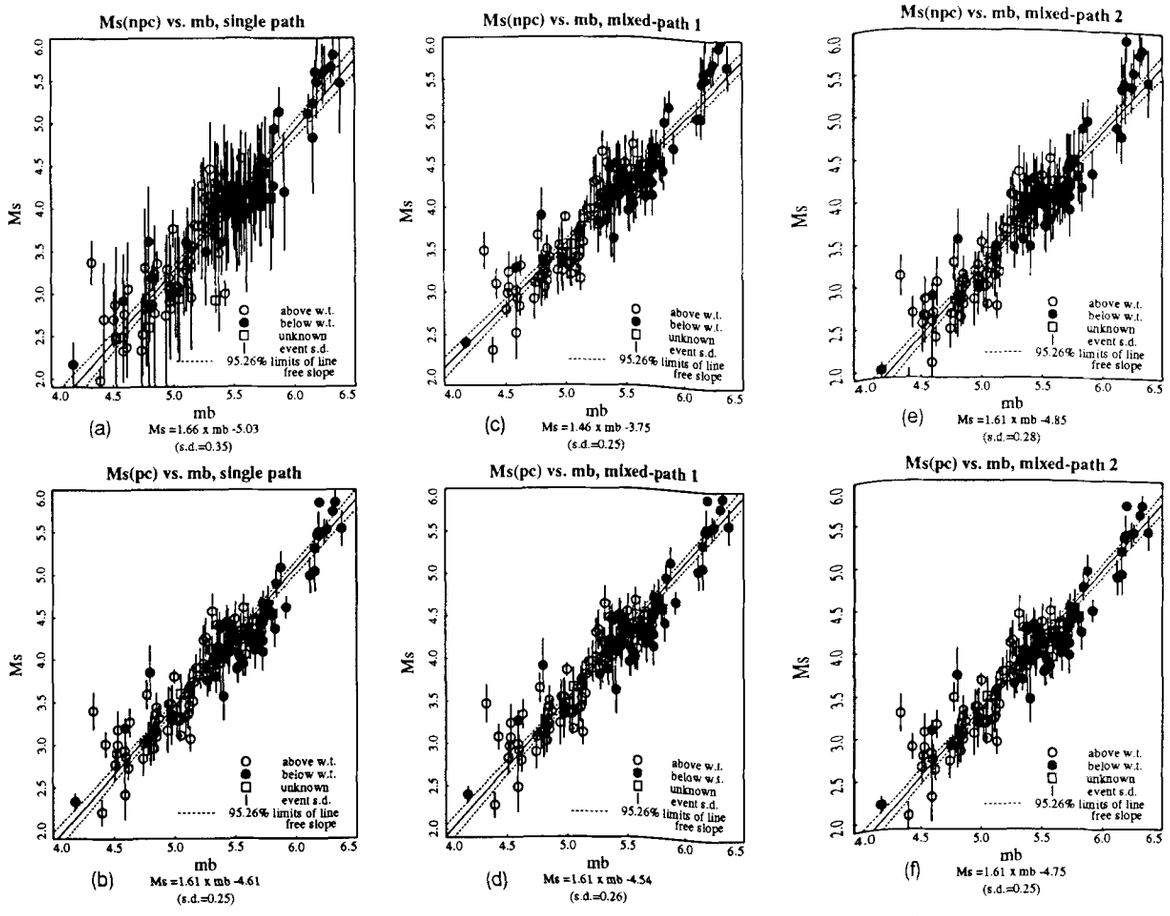

Figure 7. Here M_S is plotted versus Lilwall m_b's. For the left figures M_S is calculated with single-path Green's functions, without path corrections (npc) and with path corrections (pc). The best-fitting regression model is the solid line running through the data points. The dashed lines are the two-sigma confidence intervals of the line. The M_S–m_b relationship and the rms error of the data are at the bottom of each figure. The middle figure M_S values are determined using the mixed-path-1 synthetics and in the right two figures mixed-path-2 Green's functions were used.

waves propagated along a TNA path for 40° will be significantly more attenuated than waves propagated along a craton or shield path for that same distance. Path corrections reduce this effect significantly for the single-path derived magnitudes. Table 1 lists these network-path corrections. The third column lists the corrections for single-path synthetics. A positive value denotes that the M_S for a station is smaller than the network theoretical average.

We next explored the effect of mixed-path transfer functions upon the M_S calculations. As described above, we chose the path to RSSD as a generic structure for the second portion of the mixed-path synthetic seismogram calculations. We generate two sets of these synthetics. The difference between these two mixed-path earth structures is their spectral attenuation coefficients, with $\gamma(\omega)$ being twice as large, at a given frequency, for the mixed-path-2 case as for the mixed-path-1 case. Fig. 8 is a plot of the attenuation factor ($\gamma(\omega)$) as a function of period. The line labelled RSSD × 2 is that of the increased attenuation model. It is referred to as 'mixed-path 2' throughout this study. The lower, dashed curve is the attenuation curve for the RSSD structure. Synthetics made with this RSSD generic structure for the latter portion of the 40° travel path will be referred to as 'mixed-path 1'. Table 1 gives the path corrections for each station for these two cases, also.

The network averages and their standard deviations for the three different path assumptions are

Single path

$$M_S(PPA) = \log M_0 - 11.50, \tag{14}$$

with a standard deviation of 0.38.

Mixed-path 1

$$M_S(PPA) = \log M_0 - 11.44, \tag{15}$$

with a standard deviation of 0.17.

Mixed path 2

$$M_S(PPA) = \log M_0 - 11.64, \tag{16}$$

with a standard deviation of 0.22.

These standard deviations are only a measure of the spread of the theoretical network path corrections for a given moment. The above standard deviations could also be found from squaring and summing the path-correction values in their respective columns in Table 1 after removing the three digital stations that have the same correction as

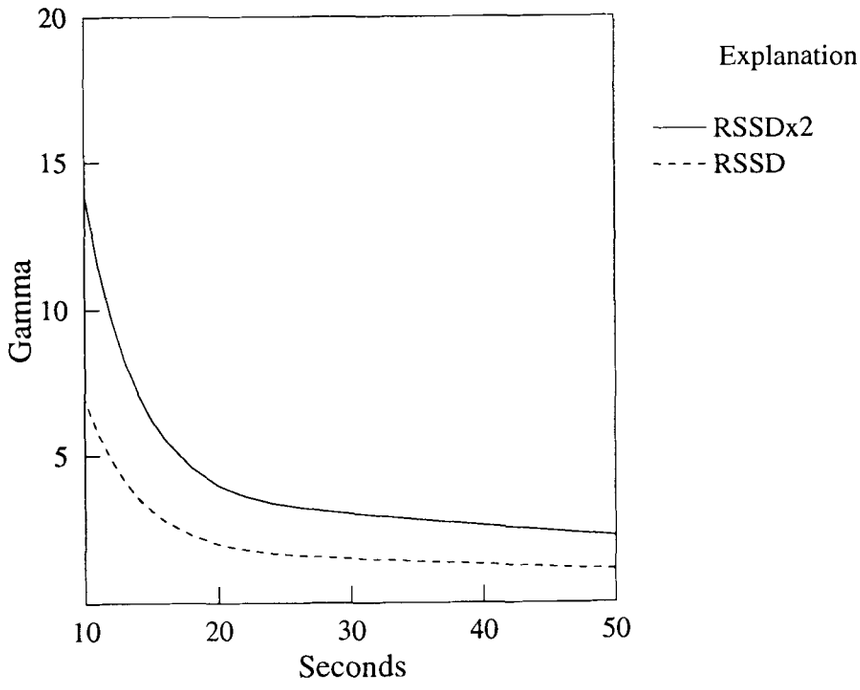

Figure 8. The two attenuation models for the generic portion of the hybrid propagation model are plotted versus period. Gamma is the attenuation coefficient (eq. 1) at a given period. Model RSSD × 2's attenuation is twice that of the RSSD model. M_S values calculated with synthetics using model RSSD are referred to as mixed-path 1, while values determined from synthetics created using attenuation model RSSD × 2 are referred to as mixed-path 2.

their analogue entries. It should be remembered that the 40° M_S were all calculated using the same WWSSN long-period instrument response and thus the path corrections are instrument-independent. In relating theoretical station amplitudes to M_S, the actual station instrument response is removed. The previously discussed regression constant of 11.43 for the entire data set differs slightly from the theoretical network value of 11.44 given in eq. (15) primarily because the individual observed values are not always determined using the full network of stations.

In Figs 7(c) and (d) the M_S magnitudes were calculated using synthetic seismograms using the mixed-path-1 model. In Fig. 7(c) the M_S's are calculated without path-correction terms, while in Fig. 7(d) path corrections are included. The addition of the path-correction terms cuts the data variance, but by no more than 25 per cent, and then not in all cases. Assuming a fixed-slope regression ($m = 1.50$), there is no offset in the intercept between the uncorrected and path-corrected M_S's. So using a generic structure for the remainder of the 40° path acts as a path correction as well.

Figures 7(e) and (f) are M_S versus m_b plots for the mixed-path-2 case without and with path corrections, respectively. It should be noted that the slope of the regression line is nearly the same (1.61) for all three path-corrected cases (Figs 7b, d and f) and that the difference in the regression intercept between the three cases is essentially what one would predict from the three theoretical network intercepts given in eqs (14), (15) and (16). This should not be surprising since the determined moment for each event is the same from figure to figure and on average their slopes should be equal and the differences in M_S between the three figures should be close to the difference in the theoretical network values. If explosions at only one site are plotted, the slope of the curve is closer to 1.5, so that we will take the M_S–m_b scaling relationship to be:

$$M_S = 1.50 \times m_b + B. \tag{17}$$

For this fixed-slope scaling relationship, the uncorrected and path-corrected mixed-path-1 M_S curves have the same intercept, whereas for the mixed-path-2 case the intercept is 0.10 units larger for the path-corrected curve than for the uncorrected curve. For path-corrected M_S's, the mixed-path-1 intercept is 0.21 log units greater than that of the mixed-path-2 curve. Because mixed-path synthetics are propagated to 40° along a more attenuative path, the M_S measured also will be smaller.

For the single-path case, path-corrected M_S values give the same relationship (slope = 1.61), but the slope is larger (1.66) for the uncorrected magnitudes, although the difference lies within the errors bounds. It would seem that both path corrections and mixed-path Green's functions improve M_S determinations for the method used here. The most consistent, reliable magnitudes are obtained using mixed-path-generated synthetics in conjunction with path corrections for the 40° M_S measurements. The variance among the mixed-path-based M_S values for the network is smaller than that when M_S is derived from single-path synthetics, so that magnitude measurements will be more consistent when they are determined from mixed-path synthetics. This is particularly important for events with few reporting stations. All further plots of M_S in this study use values obtained from the mixed-path-1 case with path corrections, unless stated otherwise.

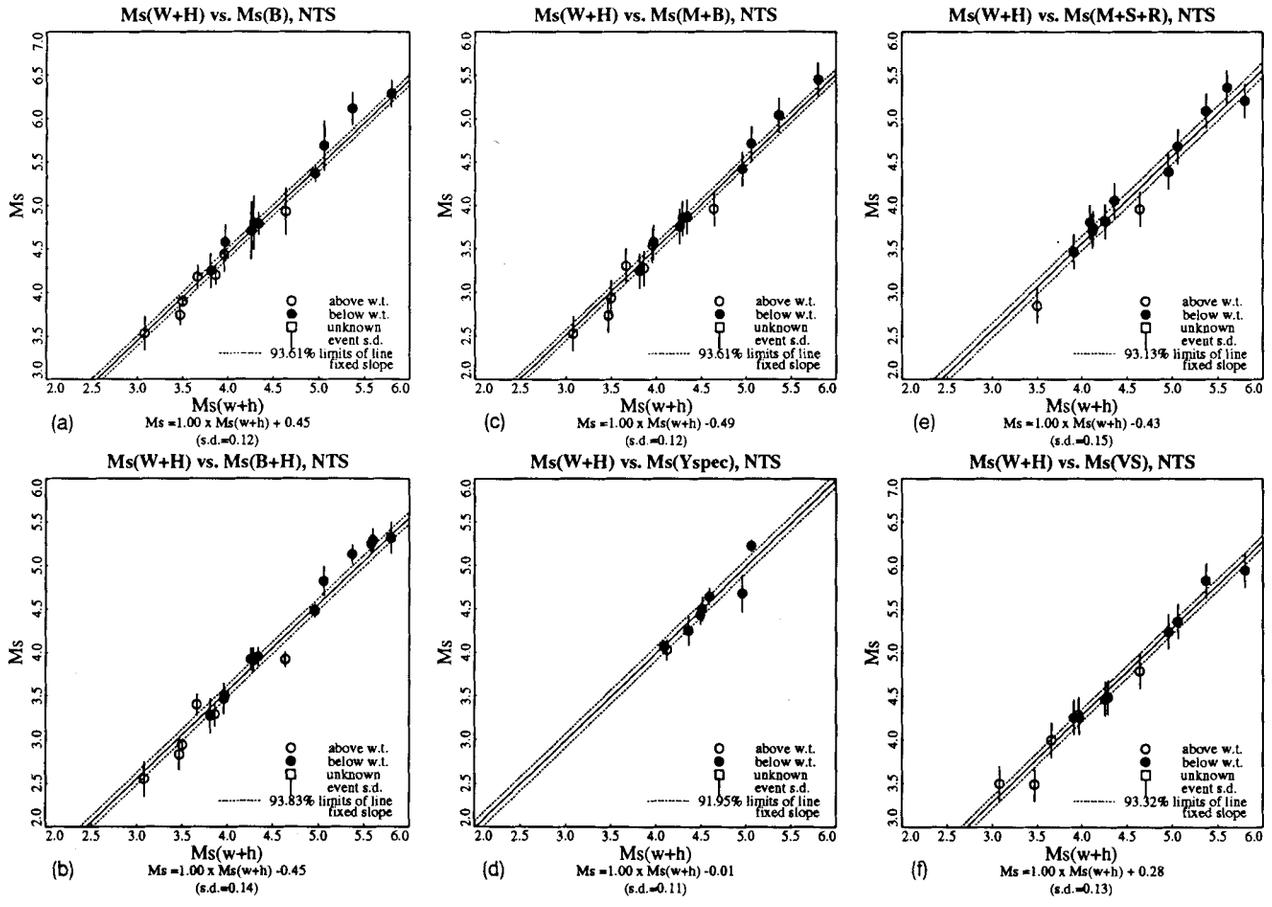

Figure 9. M_S of this study regressed against those determined by other studies.

How well the final M_S values reflect the actual seismic magnitude of these events necessitates having another measure of their size. In the event of anomalously high or low seismic-source coupling, for example, both body waves and surface waves should be affected similarly by coupling effects. A magnitude parameter independent of seismic observations would be useful to plot the M_S against, so we have also fitted our results to estimate log yields. These relationships are shown and discussed later in the paper. Yield values are estimated to be within 10 per cent of the actual yield (Springer & Kinnaman 1971). Yield information was available for 174 of the events, thus yields make up the most comprehensive data set with which to compare our results. The yields for this data set range over three orders of magnitude in size. The greatest scatter, as in the case of m_b versus log yield, is due to shots above the water table. It should also be kept in mind that the scatter would be further reduced if the data were separated into populations based on their location at NTS (i.e. Pahute Mesa, Rainier Mesa and Yucca Flat).

Since our magnitude values are based on theoretical continental structures, as well as the particular network used, we wanted to compare our M_S values to those obtained from more standard M_S methods. In addition, the reference distance of 40° is arbitrary and along with differing magnitude formulae will result in an offset from previous studies. In order to make it possible for readers to convert our values to the results of others, we regressed on magnitudes of mutual events. Fig. 9 shows our M_S values (x axis) versus those from six other studies (y axis) (Basham 1969; Marshall & Basham 1972; Marshall *et al.* 1979; Basham & Horner 1973; Yacoub 1983; von Seggern 1973). The overlap in data sets varies between 8 and 16 events. We performed a fixed-slope (slope = 1.0), linear regression of our M_S values to those of the six outside studies; in general the correlation is very good. It is important to note that with our method we are able to measure M_S for events one tenth the size of the smallest events measured in the other studies (i.e. $M_S = 1.75$ to 2.0). This is after having corrected for differences in absolute M_S scales. We are able to measure M_S for these smaller events because we are able to make use of near-regional (<500 km) records with the method described in this paper.

The offsets in M_S values vary considerably. This offset is due in part to the difference in definition of M_S for each study, in particular the distance-correction term. As discussed earlier, we chose the distance-correction term $(1.08 \times \log(\Delta))$, whereas the other studies use a variety of terms. Yacoub (1983) and Basham (1969) use variations of the Prague formula: $(1.66 \times \log(\Delta))$ Båth (1967). von Seggern (1973) used a slightly smaller distance factor $(0.9 \times \log(\Delta))$ than that of his later study which we use. The other three studies use distance corrections developed by Marshall & Basham (1972) and all are approximately

0.45 magnitude units smaller than ours. If we had used the Prague formula at a distance of 40°, our magnitudes would have been only 0.15 units smaller. The difference in distance-correction factor is believed to be the primary cause of the offset in magnitude between their results and ours. Our distance correction is also dependent upon the generic path structure chosen to generate the 40° synthetics.

These three studies, as well as that of Basham (1969), use mostly, if not all, data recorded at Canadian stations; thus their networks have strong azimuthal and distance biases as well, which may also affect magnitude measurements. It should be noted that the method described in this study to calculate M_S also is based upon a theoretical network average M_S, so it will have a bias attached to it which is dependent upon the network used. This network bias may be responsible for part of the offset, as well. Our network does have considerably better azimuthal coverage than these other studies, so that tectonic-release effects upon the long-period radiation, assuming strike-slip faulting, should be mitigated, thus giving more accurate M_S measurements.

A significant difference between our M_S calculations and those of the other studies is that we include data from close-in stations. Since the 40° synthetics used to calculate M_S travel further along an arbitrary path model for these nearer stations, it is important to consider whether or not our M_S values have some functional dependence upon distance. Fig. 10(a) plots relative station M_S versus distance for the entire data set. No apparent distance dependence is observed. We also examined this relation for individual events and found the evidence more compelling that there is no distance dependence for the M_S values, which makes this M_S method very attractive, particularly for small events, for which Rayleigh wave amplitudes are measurable only at near distances, since there will be no bias in magnitude values between large and small events. Fig. 10(b) shows the relative station M_S versus azimuth. There is some variation with azimuth. This is to be expected for we do not take into account tectonic release in our M_S calculations. Azimuthal variations in propagation paths, caused, perhaps, by different tectonic regions may also contribute to this effect. The potential bias due to azimuthal averaging of our network and those of previous studies is discussed in the sequel paper as a function of the orientation and strength of tectonic release at NTS.

As pointed out by an anonymous reviewer, there is no physical significance to the magnitude-offset constant, and it only matters for comparison with other studies. It was suggested that we could renormalize our M_S values, i.e. change the constant in the our modified M_S formula, eq. (9), so that they then could be used together with other M_S measurements, e.g. on an m_b versus M_S plot with earthquakes where the earthquake is determined by standard means. Unfortunately, very few explosion studies have been made using standard means. We recommend the use of explosion moments for that purpose since they have a physical interpretation and have very few arbitrary assumptions in their determination. In this paper, we prefer to give the regression-conversion constants between the various explosion studies. They can be found in the labels on Fig. 9 but for convenience, we give them here. In order to convert our values to those of Basham (1969), add 0.45; Marshall & Basham (1972), subtract 0.49; Basham & Horner

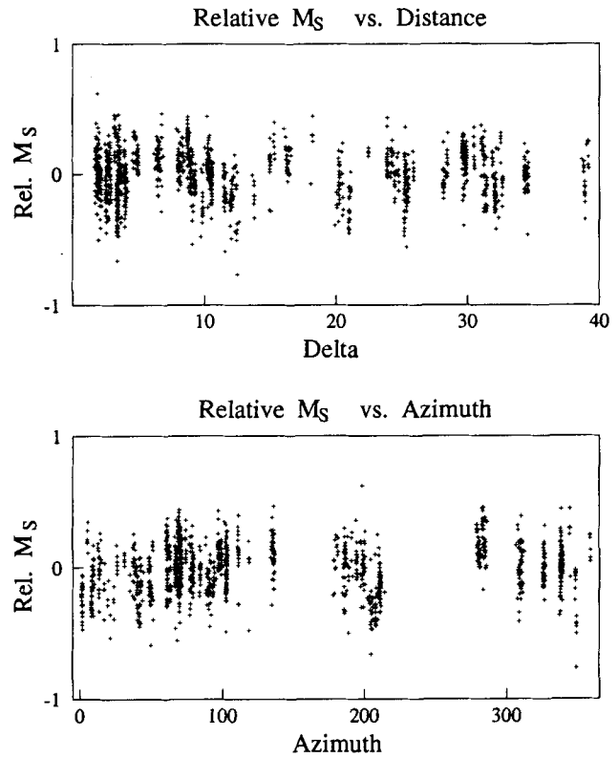

Figure 10. Relative M_S (individual station–network average) versus distance (top figure) and azimuth (bottom figure). M_S values do not appear to be a function of distance. There also is no apparent functional relationship between azimuth and M_S; some azimuths are not covered, however.

(1973), subtract 0.45; von Seggern (1973), add 0.28; Marshall *et al.* (1979), subtract 0.43; and Yacoub (1983), subtract 0.01. As an example, if we modify our regression relation between M_S and $\log M_0$ for NTS (Fig. 4) to Marshall *et al.* (1979) M_S values using the above, we obtain $M_S = \log M_0 - 11.85$. This is in fair agreement with the observation by Stevens & McLaughlin (1986) that $M_S = \log M_0 - 12.00$ fit well for NTS, Novaya Zemla and Amchitka explosions using Marshall *et al.* (1979) M_S values for NTS and Amchitka. Only six NTS events were on the figure showing this. Later in the report, 15 NTS explosions, with 11 Marshall, Lilwall & Farthing (1986) and 4 NEIC determinations of M_S, were plotted versus $\log M_0$ and these were in much better agreement with our converted constant of 11.85 than their three-test-site value of 12.00. In Stevens (1986), it was found that 11.86 fitted his East Kazakh explosion moments using Sykes & Cifuentes (1984) M_S values for the 10 events they had in common.

Table 2 lists the final mixed-path-1, path-corrected M_S values for the 190 events of this study. The first column lists the number of stations recording the event. Next the surface-wave magnitude and associated error for the event are given. This is followed by a three-letter shot-information code. The first letter denotes its geographic location: Yucca (Y), Pahute (P), Rainer (R), or Climax Stock (C). The second is whether its shot depth was above (A) or below (B) the water table. The last letter describes the shot-site rock as tuff (T), rhyolite (R), granite (G), or alluvium (A). An underscore means that the information is not known.

Table 2. Event information.

No. Sta.	M_S	M_S s.e.	Shot Info.	Event	Julian Date	No. Sta.	M_S	M_S s.e.	Shot Info.	Event	Julian Date
1	2.49	-	R__	Rainier	57262	5	3.86	0.04	YAT	Yard	67250
1	3.25	-	R__	Logan	58289	1	2.08	-	YAA	Marvel	67264
1	3.73	-	R__	Blanca	58303	9	3.64	0.05	YBT	Cobbler	67312
1	2.96	-	NBG	Hardhat	62046	10	5.40	0.06	NBT	Faultless	68019
1	2.89	-	YAA	Dormouseprime	62095	6	3.53	0.05	RAT	Dorsalfin	68060
1	3.57	-	YA_	Aardvark	62132	4	2.85	0.06	N__	Buggy1	68072
1	3.12	-	YAA	Haymaker	62178	3	5.80	0.01	PBR	Boxcar	68117
1	3.69	-	YAA	Sedan	62187	10	4.75	0.09	PAT	Rickey	68167
1	3.66	-	YA_	Mississippi	62278	11	4.48	0.06	PAR	Chateaugay	68180
2	4.85	0.22	YBT	Bilby	63256	9	3.43	0.08	RAT	Hudsonseal	68268
1	3.77	-	RAT	Clearwater	63289	1	3.14	-	YAA	Crew	68309
2	3.07	0.28	YAL	Handcar	64310	4	3.66	0.10	PAT	Schooner	68343
2	2.54	0.08	YAA	Merlin	65047	4	5.92	0.08	PBT	Benham	68354
1	2.82	-	NAA	Wishbone	65049	11	4.03	0.05	RAT	Wineskin	69015
12	3.97	0.06	YBT	Wagtail	65062	1	3.20	-	RAT	Cypress	69043
6	3.96	0.07	YAT	Cup	65085	15	4.06	0.04	YBT	Blenton	69120
1	2.59	-	PAR	Palanquin	65104	9	5.58	0.05	PBT	Jorum	69259
4	2.40	0.06	PBT	Buteo	65132	9	4.68	0.05	PAR	Pipkin	69281
4	3.08	0.09	NAA	Dilutedwaters	65167	3	2.11	0.06	YAT	Cruet	69302
7	3.66	0.05	YAT	Charcoal	65253	3	2.53	0.12	YAT	Pod	69302
5	3.81	0.09	YBT	Lampblack	66018	4	4.36	0.14	YBT	Calabash	69302
8	3.91	0.12	PBT	Rex	66055	2	3.17	0.02	R__	Dieseltrain	69339
13	3.96	0.07	PAR	Duryea	66104	2	3.34	0.05	RAT	Dianamist	70042
5	3.47	0.11	NAT	Pinstripe	66115	2	3.46	0.05	YAT	Cumarin	70056
3	2.81	0.05	YAA	Cyclamen	66125	2	3.22	0.18	YAA	Yannigan	70057
11	4.01	0.10	PAR	Chartreuse	66126	3	2.14	0.24	YAT	Cyathus	70065
15	4.34	0.04	YBT	Piranha	66133	3	1.66	0.20	YAT	Arabis	70065
6	3.50	0.06	YAT	Discusthrower	66147	2	2.22	0.27	YAA	Jal	70078
26	4.27	0.04	CBG	Piledriver	66153	17	4.29	0.05	YBT	Shaper	70082
18	4.29	0.03	YBT	Tan	66154	8	5.56	0.08	PBT	Handley	70085
3	2.70	0.13	YAA	Vulcan	66176	5	3.35	0.13	RAT	Mintleaf	70125
3	5.06	0.15	PBR	Halfbeak	66181	7	3.76	0.08	YAT	Cornice	70135
3	5.37	0.11	PBT	Greeley	66354	13	3.54	0.06	YAT	Morrones	70141
2	2.39	0.05	YAA	Ward	67039	2	1.79	0.33	YAT	Manzanas	70141
1	2.38	-	YAA	Persimmon	67053	5	3.12	0.06	RAT	Hudsonmoon	70146
5	4.55	0.09	YAA	Agile	67054	16	4.12	0.07	YAT	Flask	70146
7	4.96	0.06	YBT	Commodore	67140	2	2.40	0.10	YAA	Embudo	71167
10	4.64	0.07	PAR	Knickerbocker	67146	4	3.01	0.09	YAT	Laguna	71174
3	3.46	0.05	RAT	Midimist	67177	4	3.21	0.02	YAT	Harebell	71175
2	3.03	0.14	RAT	Doormist	67243	10	3.16	0.06	RAT	Camphor	71180
15	4.13	0.03	YBT	Miniata	71189	11	4.40	0.05	YAT	Baseball	81015
21	3.63	0.06	YBT	Algodones	71230	10	4.18	0.07	YBT	Rousanne	81316
2	2.59	0.06	YAT	Pedernal	71272	9	4.67	0.05	YBT	Jornada	82028
4	2.59	0.04	YAT	Cathay	71281	10	4.52	0.06	PBR	Molbo	82043
4	2.29	0.17	YAA	Longchamps	72110	8	4.41	0.08	PAR	Hosta	82043
7	3.44	0.10	RAT	Mistynorth	72123	4	2.99	0.10	YAT	Tenaja	82107
5	3.27	0.06	YBT	Monero	72140	6	4.44	0.05	PAT	Gibne	82115
7	3.35	0.06	RBT	Diamondsculls	72202	15	4.29	0.04	YBT	Bouschet	82127
1	2.50	-	YA_	Delphinium	72270	9	4.52	0.05	PAR	Nebbiolo	82175
12	4.09	0.04	YBT	Miera	73067	9	3.04	0.10	YAT	Monterey	82210
22	4.09	0.03	YBT	Starwort	73116	9	4.73	0.05	YBT	Atrisco	82217
8	3.35	0.08	RAT	Didoqueen	73156	8	3.38	0.05	RAT	Huronlanding	82266
5	5.10	0.12	PBR	Almendro	73157	5	3.54	0.11	RAT	Frisco	82266
15	4.35	0.05	YBT	Latir	74058	2	2.49	0.29	YAA	Seyval	82316
8	3.43	0.08	RAT	Mingblade	74170	6	3.13	0.09	YAA	Manteca	82344
20	4.59	0.05	YBT	Escabosa	74191	2	1.80	0.01	YAA	Cerro	82245
13	3.96	0.05	YBT	Stanyan	74269	3	2.52	0.08	YBT	Borrego	82272

Table 2. (*Continued.*)

No. Sta.	M_S	M_S s.e.	Shot Info.	Event	Julian Date	No. Sta.	M_S	M_S s.e.	Shot Info.	Event	Julian Date
15	4.02	0.04	YBA	Cabrillo	75066	11	4.01	0.05	PAR	Cabra	83085
3	3.24	0.18	RAT	Diningcar	75095	20	4.15	0.05	YBT	Torquoise	83104
13	3.74	0.05	YBT	Obar	75120	7	2.83	0.07	YAA	Crowdie	83125
10	4.65	0.06	PBR	Stilton	75154	12	3.34	0.05	YAT	Fahada	83146
23	4.51	0.06	YBT	Mizzen	75154	10	2.93	0.06	YAA	Danablu	83160
3	5.53	0.02	PBT	Camembert	75177	12	4.17	0.06	PAR	Chancellor	83244
1	3.37	-	RAT	Huskypup	75297	3	3.04	0.22	R__	Midnitezephyr	83264
4	5.59	0.07	PBT	Kasseri	75301	5	2.50	0.04	YBT	Techado	83265
3	5.91	0.02	PBT	Muenster	76003	11	3.81	0.06	YAT	Romano	83350
14	4.49	0.05	YBT	Keelson	76035	9	3.42	0.06	RAT	Midasmyth	84046
8	5.56	0.09	PBT	Fontina	76043	1	2.28	-	YAA	Agrini	84091
13	5.15	0.05	PBR	Cheshire	76045	19	4.40	0.04	YBT	Mundo	84122
6	5.62	0.11	PBT	Colby	76074	11	4.48	0.06	YBT	Caprock	84152
3	3.23	0.17	RAT	Mightyepic	76133	4	3.16	0.17	YAT	Duoro	84172
8	4.24	0.05	YBT	Rudder	76363	21	4.18	0.07	PAR	Kappeli	84207
18	4.17	0.04	YBT	Bulkhead	77117	6	2.90	0.09	YAT	Correo	84215
10	4.09	0.05	YBT	Crewline	77145	3	3.08	0.03	YAT	Dolcetto	84243
27	4.29	0.04	YBT	Lowball	78193	5	3.58	0.08	YAT	Breton	84257
4	3.12	0.17	R__	Diablohawk	78256	4	2.80	0.08	YAA	Villita	84315
13	3.87	0.05	YBT	Quargel	78322	12	4.23	0.06	PAT	Egmont	84344
21	4.35	0.04	YBT	Quinella	79039	14	4.22	0.06	PAR	Tierra	84350
22	4.14	0.05	YBT	Pyramid	80107	11	4.43	0.07	YBT	Tortugas	84061
6	3.36	0.13	RAT	Minersiron	80305	5	3.39	0.06	YAT	Vaughn	85074
4	4.03	0.23	YAT	Cottage	85082	10	4.42	0.07	PAR	Cybar	86198
8	4.72	0.08	YBT	Hermosa	85092	2	2.97	0.02	YAA	Cornucopia	86205
7	3.47	0.12	R_T	Mistyrain	85096	8	4.29	0.07	PAR	Labquark	86273
19	4.37	0.06	PBT	Towanda	85122	7	4.34	0.05	P__	Belmont	86289
13	4.46	0.05	PBR	Salut	85163	5	4.58	0.07	YBT	Gascon	86318
12	4.30	0.05	PAR	Serena	85206	7	4.55	0.08	P__	Bodie	86347
4	3.24	0.13	YAT	Ponil	85270	4	4.38	0.10	P__	Delamar	87108
8	4.19	0.09	YBT	Kinibito	85339	8	4.47	0.07	PAT	Hardin	87120
8	4.19	0.06	P__	Goldstone	85362	4	3.66	0.14	Y__	Midland	87197
4	4.07	0.06	YBT	Glencoe	86081	5	4.60	0.08	Y__	Tahoka	87225
7	3.40	0.09	RAT	Mightyoak	86100	4	4.51	0.13	P__	Lockney	87267
12	4.33	0.07	PAR	Jefferson	86112	3	3.87	0.06	Y__	Borate	87296
2	2.53	0.12	YAA	Panamint	86141	1	4.09	-	PAT	Kernville	88046
7	4.22	0.10	YAT	Tajo	86156	1	4.17	-	PAT	Kearsarge	88230
15	4.31	0.05	P__	Darwin	86176	1	3.36	-	Y__	Kawich	89055

The final two columns give the name and Julian data of each event, respectively. The events are listed in chronological order. The error listed is the standard deviation of the mean or standard error and the standard deviation of the observations can be obtained by multiplying by the square root of the number of observations or stations used. The average standard deviation for the list is 0.15. It is questionable as to what that statistic means, however, since there are events in the table with M_S determined with only one station or infinite standard deviation, and these were obviously not used in determining the average. There are not a lot of NTS studies that give the error for M_S but the standard deviations or the more frequently used standard error of path-corrected log M_0, which is very similar to our M_S method, for NTS can be found in Stevens (1986) and Stevens & McLaughlin (1988). Stevens (1986) notes that the network standard deviations in (log) moment for his study of 40 NTS events are quite small, about 0.1, and that even for recent NTS explosions, which included data from several distant SRO stations, the standard deviations are only 0.15.

To determine the portability of this M_S calculation method the events need to be separated into groups based on their source regions and then compared, one group to another, in order to see if there are systematic differences in M_S values relative to any other magnitude scale. Three main geographic source regions comprise the event data set: Pahute Mesa, Rainier Mesa and Yucca Flat.

Whether or not a shot occurs within saturated material is another criterion by which to separate events in order to look for systematic differences in M_S values. Other studies have found significant seismic-coupling differences between explosions detonated above and below the water table (Marshall *et al.* 1979; Gupta *et al.* 1989; Vergino & Mensing 1989). It is important to quantify this seismic-coupling effect.

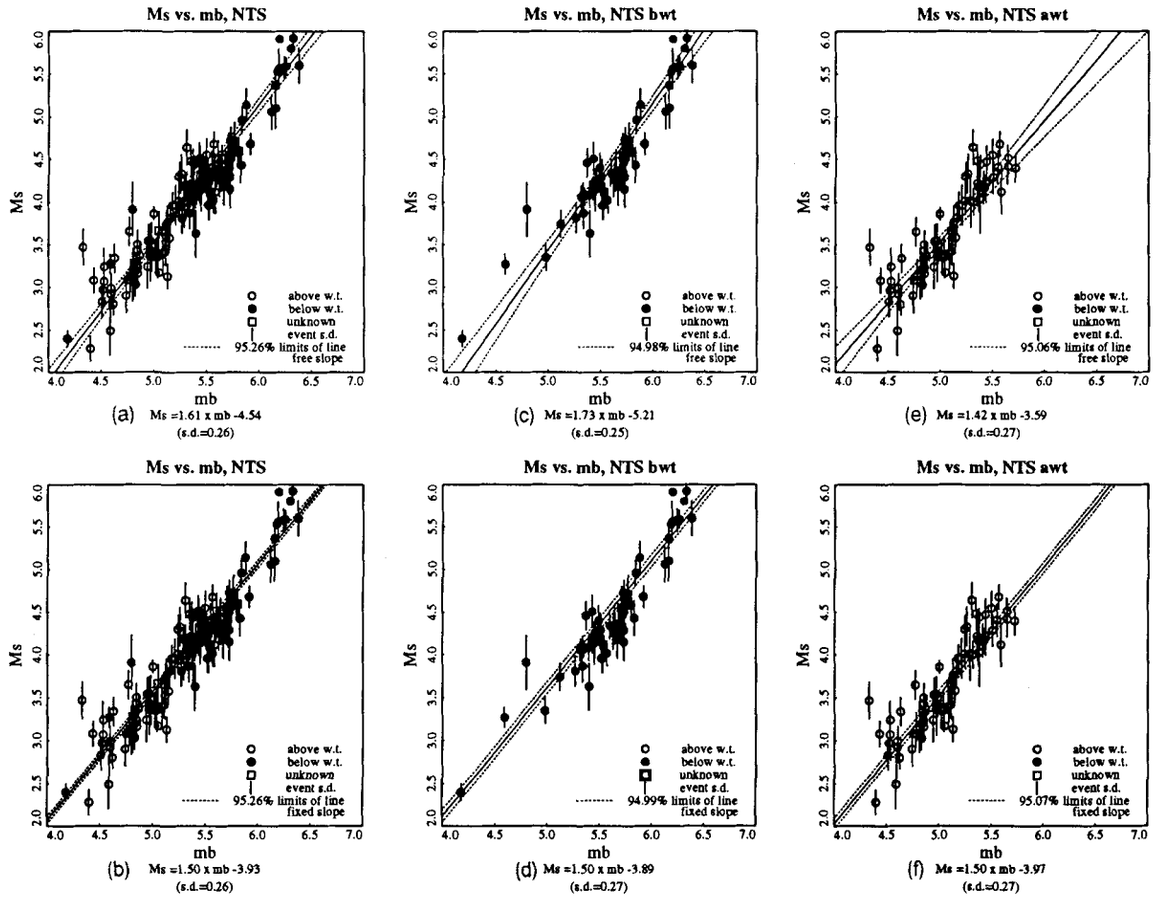

Figure 11. M_S regressed versus Lilwall m_b for all NTS events. The data are also separated with respect to shot point being above or below the water table. The bottom figures are constrained least-square regressions assuming a slope of 1.5.

Reviewing Fig. 6, it is also apparent that shots fired-off below the water table have a larger body-wave magnitude than those detonated above the water table.

Figure 11(a) shows the M_S:m_b (Lilwall) relationship for all NTS events. The surface-wave magnitudes were all calculated using mixed-path Green's functions (with the RSSD-1 structure for the generic path part) and path corrections. Figs 11(b) and (c) divide the data populations into above and below the water table, respectively; shots for which water-table information was not available were left out. Although all but one Rainier Mesa events were detonated above the water level, we found that their coupling (M_S versus log yield) was diagnostic of explosions detonated below the water table. Taylor (1983) notes that Rainier Mesa sports a perched aquifer. We believe that the Rainier Mesa events are detonated within this zone, hence they are assumed to be well-coupled events, i.e. the pore space of the shot medium is filled with water and thus pore-space crushing will not be a strong effect.

The bottom three figures (11d, e and f) plot the same data, but a constrained least-squares fit was performed with the slope = 1.50. The offset in curves between events detonated above and below the water table is 0.08. This amount is within the scatter of the data (i.e. statistically insignificant), but it would appear that shot-medium coupling effects associated with pore-filling phenomena are similar for surface waves and *P* waves.

Figures 15(a)–(c) are M_S versus log-yield plots analogous to Figs 11(a)–(c). It is important to note that the individual explosion variances are about the same size for the entire range of yields, so that our predicted yield values for small events should be as accurate as for the larger events. The slope of the M_S and log-yield scaling-relation curves was found to be near unity for all populations. Assuming the scaling relationship has a slope of 1, BWT shots couple more strongly than AWT shots by 0.52 units—a substantial amount; for m_b–yield scaling the coupling effect found in this study is 0.28 units. This coupling factor depends on the slope of the scaling curve and has been found to be as large as 0.7 to 0.9 throughout the literature. For individual source regions, the offset in the M_S–yield and m_b–yield scaling curves for shots fired above and below the water table vary slightly from these values determined from the entire data set. There is some scatter in the data which is not surprising considering the diversity of the sampled populations. However the best-fitting M_S–m_b curves are well constrained, for the population covers a wide range of magnitudes.

The various M_S:m_b relationships for Yucca events are shown in Figs 12(a)–(c). The scatter in the data is reduced by 25 per cent over that of the general population (Figs

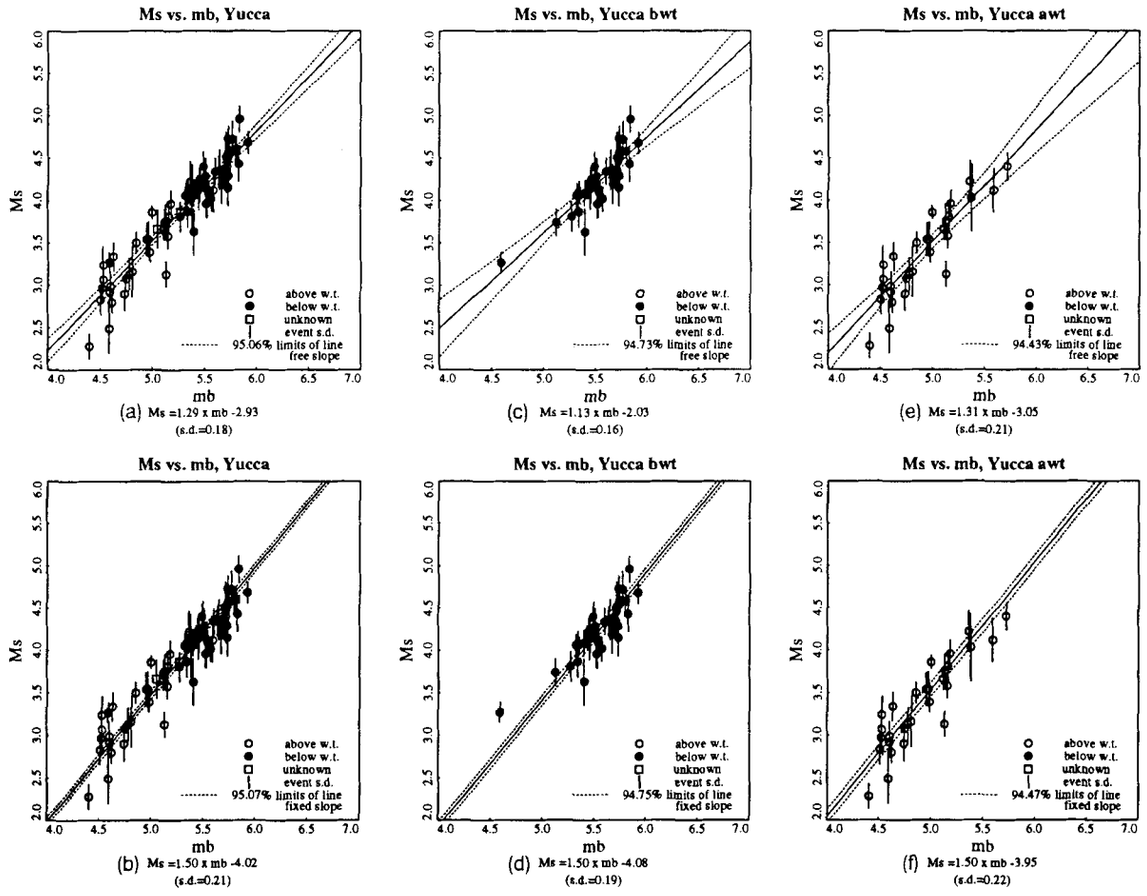

Figure 12. M_S regressed versus Lilwall m_b for Yucca events. The data are also separated with respect to shot point being above or below the water table. The bottom figures are constrained least-square regressions assuming a slope of 1.5.

11a–c). The free-slope regression curves are not as well constrained as those of Fig. 11 because the yield range for Yucca explosions is smaller than that of the entire data set. Fixing the slope to 1.5 (Figs 12d–f) leads to AWT shots coupling 0.13 M_S units more strongly than BWT shots for a given m_b. The error in the fit to the curve is larger than this variation, so it is not a statistically significant result. It would appear the pore-filling coupling affects surface wave and body waves similarly. When the Yucca M_S data are regressed with respect to log yield, as shown in Figs 15(d)–(f), it is found that BWT events couple four times more efficiently than AWT shots ($\Delta M_S = 0.61$). This is a significant amount and the data set on which it is based is more extensive than that of the M_S–m_b regression. Springer (1966) found that high dry porosity (60 per cent) shot mediums coupled four to five times less effectively than in saturated alluvium. Most Yucca Flat shots are detonated in alluvium.

Figure 13(a) plots all Pahute event M_S's versus their respective m_b's. The scaling relationship is significantly different than that of the Yucca data above. Comparing the unconstrained below- and above-water-table curves (Figs 13b and c) to their Yucca counterparts (Figs 12b and c), it is apparent that explosions at the two sites do not display the same scaling relationships. One possible explanation for this difference is that there is not enough data to constrain the scaling curves, particularly for Yucca BWT and Pahute AWT events. Another possible explanation is that this scaling relationship difference is real and may be caused by differences in the source medium, source structure or tectonic-strain release associated with the sites. Figs 12(d)–(f) and 13(d)–(f) show constrained (slope = 1.5) regression curves for the Yucca and Pahute data, respectively. For a given m_b, surface-wave magnitudes for events at Pahute Mesa are larger than those at Yucca Flat by 0.39 and 0.18 log units for BWT and AWT shots, respectively. There is also an appreciable difference in the M_S:log-yield relationship between Yucca and Pahute events detonated in water-saturated material (0.23 units). The Pahute data are plotted in Figs 16(d)–(f). For the case of events exploded in dry material there is a significant difference with Yucca events having a M_S 0.44 units smaller than Pahute events.

Figures 14(a)–(f) display the M_S–m_b regression curves and data for Rainier Mesa events in combination with and without Pahute Mesa data. Figs 16(a)–(c) are analogous figures for the M_S versus log-yield data to Figs 14(a)–(c). Although the clustering of Rainier data near $m_b = 5.0$ causes the curve to be poorly constrained, a slope is obtained that is close to that for Pahute and Yucca BWT shots. Comparison of the equations at the bottom of Figs 13(e) and 14(e) give an offset of 0.47 between M_S estimates

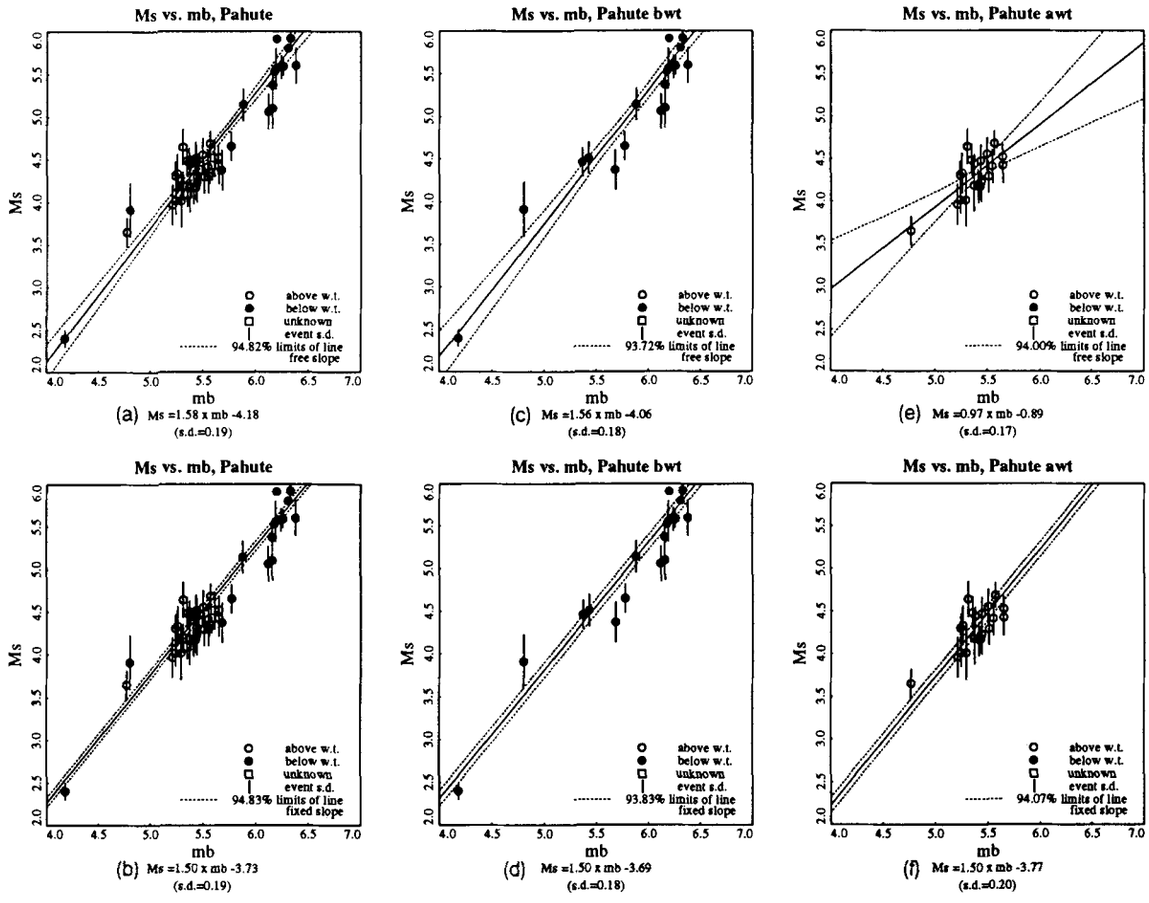

Figure 13. M_S regressed versus Lilwall m_b for Pahute events. The data are also separated with respect to shot point being above or below the water table. The bottom figures are constrained least-square regressions assuming a slope of 1.5.

at Pahute and Rainier (for a given m_b). Either the Pahute site is more efficient at producing surface waves or the Rainier site is more efficient at coupling body-wave energy. Rainier events are tunnel shots. The immediate source region ($R < 200$ m) may behave like an asymmetric cavity, resulting in a source that is non-isotropic (Zhao & Harkrider 1992) and/or seismic coupling that has strong frequency dependence. Either of these effects may account for this difference. The difference in the M_S–log-yield scaling relationship is somewhat less (0.31 units), implying that Rainier more efficiently couples short-period energy than Pahute.

Comparing Fig. 11(b) with 15(b), we see that regressing against log yield has reduced the regression standard deviation from 0.25 to 0.18 for NTS BWT events plus Rainier events. This is probably caused by the reduced standard deviation of the Pahute BWT events, 0.18 to 0.13 (Figs 13b and 16e) and the combined Pahute BWT plus Rainier events, 0.22 to 0.16 (Fig 14b and 16b). The opposite is true for the 'all' NTS events. This is because of the increase in standard deviation for Yucca AWT events when regressed against yield due primarily to the inclusion of a lot of small-yield Yucca events for which we did not have m_b's.

CONCLUSION

In this study we have determined surface-wave magnitudes for small as well as large underground nuclear explosions. Our technique allows us to include smaller events in a consistant manner with the historic set of large events for which surface-wave magnitudes have been determined by classical means. Thus it was not primarily an attempt to improve M_S for large events but to extend it to lower-sized events by including regional stations not usually used in NTS M_S determinations. The M_S formula used was one that had previously been found appropriate for NTS explosions and not the Prague formula used for earthquakes. In the process of making these determinations, we also calculated station and network moments. Since the assumptions and corrections used in the moment determinations were more straightforward, we feel that future estimates of surface-wave energy should be moment and until that time we feel that our technique is best for including small events in the historical surface-wave magnitude data base. The moment values will be given in the sequel paper.

The method we have described to calculate surface-wave magnitudes allows the measurement of M_S for nuclear explosions over a wider magnitude distribution than was

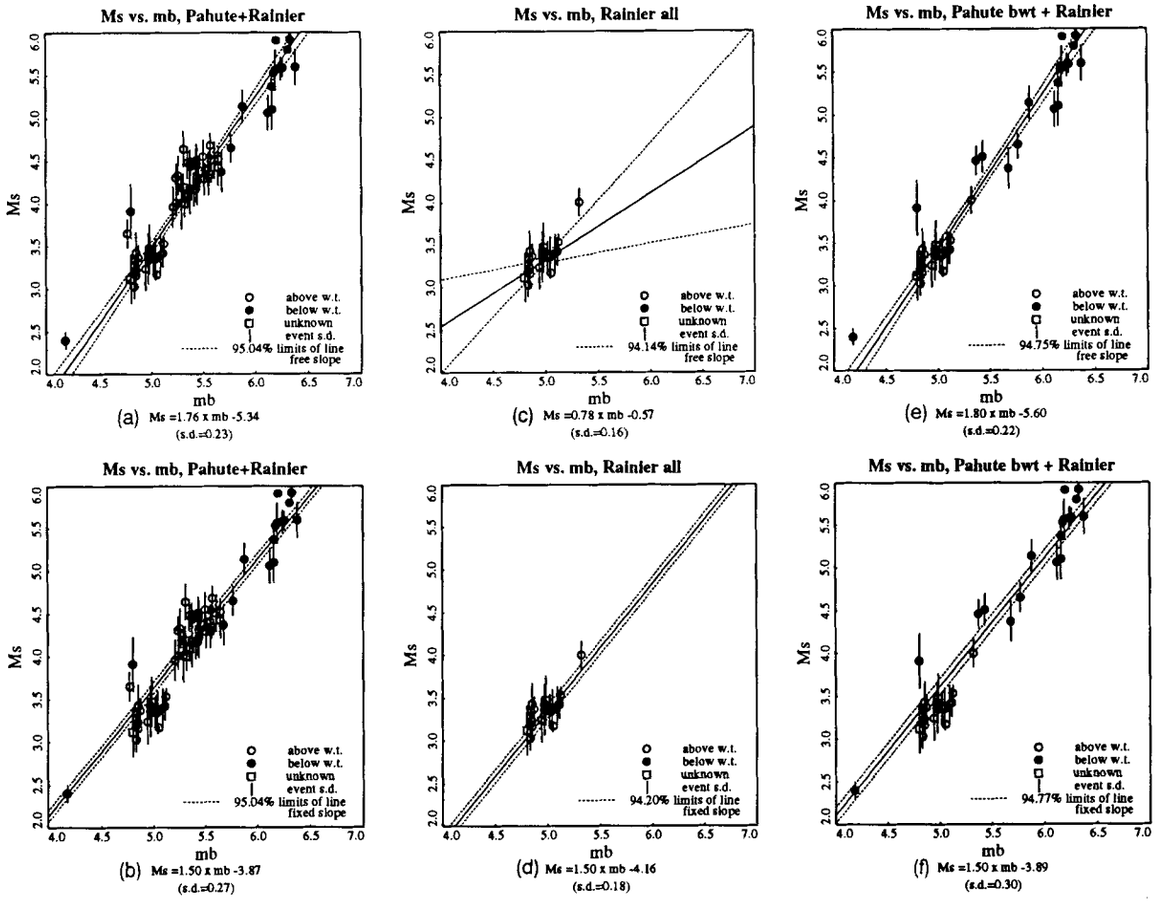

Figure 14. M_S regressed versus Lilwall m_b for Pahute and Rainier events. Regression of Rainier data alone (middle figures), all Rainier and Pahute events (left figures), and all Rainier events with Pahute shots below the water table (right figures) are shown. The bottom figures are constrained least-square regressions assuming a slope of 1.5.

previously possible. These M_S values scale consistently (within a constant factor) with other seismic-magnitude scales. Using our technique, it is now possible to use near-regional ($\Delta < 8°$) long-period records, as well as more conventional far-regional ($\Delta < 15°$) and teleseismic observations, in order to measure surface-wave magnitudes. As it is a time-domain measurement, it is easy to calculate M_S from historical analogue waveforms, since it is only necessary to measure the peak-to-peak Rayleigh wave amplitude.

This M_S method is very useful for quantifying small explosions, because time-domain magnitude measurements of regional waveforms lowers the effective magnitude threshold. Small events, for which teleseismic surface waves are not observed, can now be analysed with regional surface-wave data, thus lowering the effective measuring M_S threshold. Fig. 17 illustrates this point, showing unrotated three-component data for FLOYDADA (8/15/91, $m_b = 4.2$) detonated at Yucca Flat and recorded by three TERRAscope stations convolved with a Press–Ewing 30–90 response. The source-to-receiver distances are between 210 and 390 km. The maximum peak-to-peak amplitudes are quite small (<0.5 mm). On the actual analogue instrument it would not be possible to measure the surface-wave amplitude. Because of the low signal-to-noise ratio a spectral moment would be of dubious value. However, the M_s and M_0(PPA) methods described in this paper would furnish an accurate surface-wave magnitude with which to estimate its yield.

These small surface-wave magnitudes, based on near-regional data would also be of considerable value for discrimination methods that make use of the difference between the long-period and short-period spectral content of earthquakes and explosions, for it is possible to lower the discrimination threshold using such data.

The increase in nearer observations has several other advantages. Station-network coverage is enhanced in terms of overall numbers as well as in azimuthal coverage. In this study stations a few hundred kilometers away from NTS in the south-western U.S. were included in the network that otherwise would have no coverage to the west or south-west. These improvements make the network M_S's more stable and statistically robust. Potential monitoring areas may well have similar geographical constraints requiring the use of near-regional ($\Delta < 8°$) seismic data. Also, the effect of inaccuracies in estimating Q are negligible for very near-regional recordings.

From the results obtained with the data set used here, there do appear to be significant differences in seismic

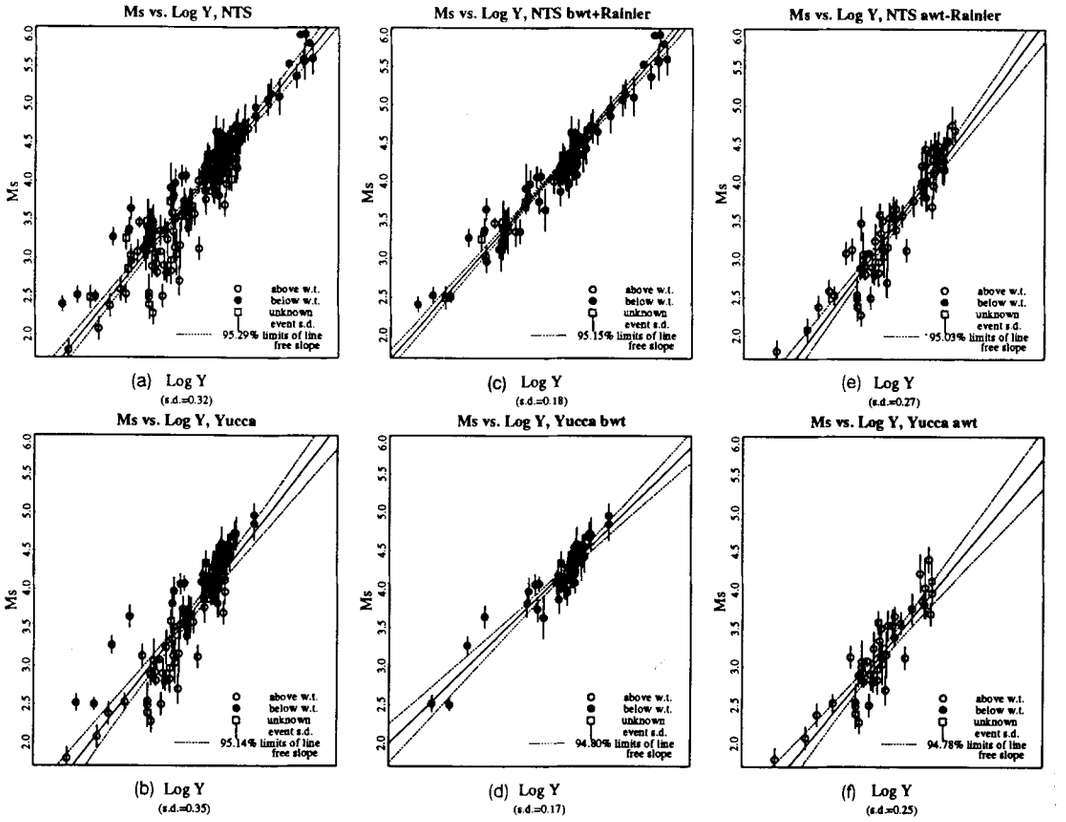

Figure 15. M_S regressed versus log yield for all NTS events (top figures) and for Yucca events (bottom figures). Event populations have also been grouped with respect to shot-point water-table location.

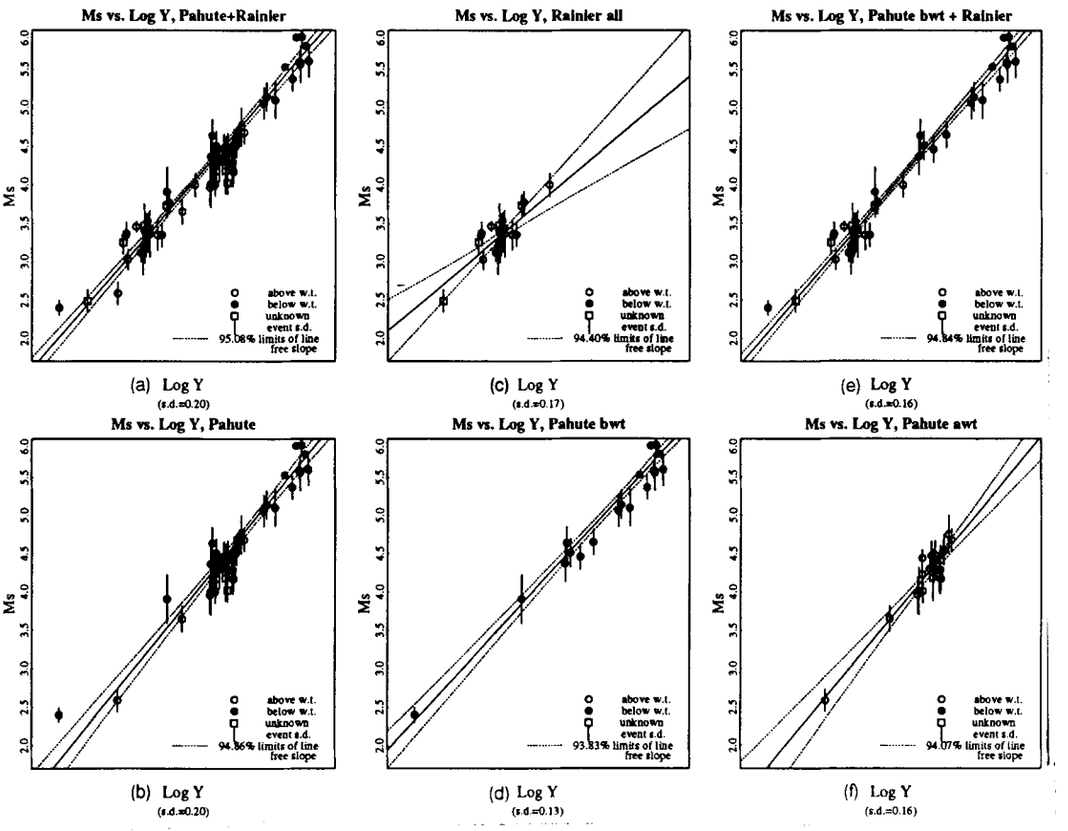

Figure 16. M_S regressed versus log yield for Pahute and Rainier events (top figures) and for Pahute events alone (bottom figures). Event populations have also been grouped with respect to shot-point water-table location.

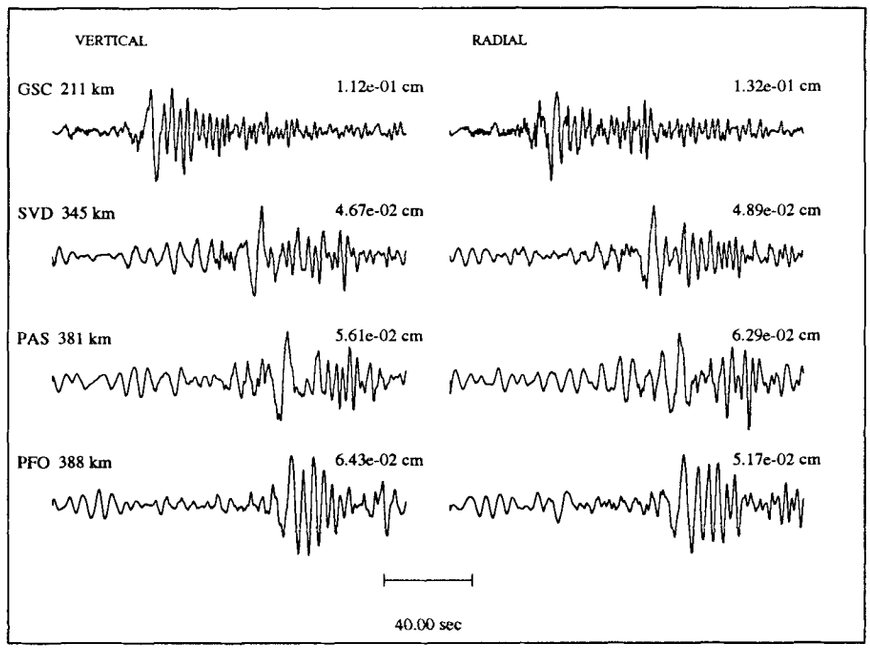

Figure 17. TERRAscope streckeisen recordings of an NTS explosion Floydada at Yucca Flat on 8/15/91 with an estimated yield of <10 kt. ($m_b = 4.2$, $M_L = 4.0$, and $\log M_0 = 14.16$ N–M). The broad-band records have been convolved with a Press–Ewing 30–90 instrument response. All four stations record the surface wave train well enough to measure the Airy-phase peak amplitudes. Records from an actual 30–90 long-period instrument would be unusable.

coupling between NTS subsites, with events at Pahute Mesa producing larger surface-wave magnitudes for a given m_b than at Rainier Mesa or Yucca Flat. For well-coupled events this discrepancy is largest for Rainier Mesa events. M_S values at Yucca Flat tend to be larger than those at Rainier Mesa by 0.08 magnitude units for a given m_b. There also appears to be some difference in waveforms between events of these two source regions. Pahute Mesa events are 0.39 magnitude units larger than those at Yucca flat for explosions set off below the water table and with the same m_b.

Although L_g measurements with a calibration shot give more accurate estimates of explosion yields, there may be cases where L_g 'blockage' caused by strong lateral variations in the propagation path may occur, and one must use other methods, such as surface-wave magnitudes, to estimate yields or for discriminating the event.

ACKNOWLEDGMENTS

This research was supported by the Defense Advanced Research Projects Agency (DOD), Nuclear Monitoring Research Office and was monitored by Air Force Geophysics Laboratory under Contract F19628-89-K-0028, and also was supported by Phillips Laboratory (formerly Geophysics Laboratory) of the Air Force Systems Command under Contract F19628-90-K-0049, and contribution No. 5187, Division of Geological and Planetary Sciences, California Institute of Technology, Pasadena, California.

REFERENCES

Alewine, R.W., 1972. Theoretical and observed distance corrections for Rayleigh-wave magnitude, *Bull. seism. Soc. Am.*, **62,** 6133–6142.

Babich, V.M., Chikhachev, B.A. & Yanovskaya, T.B., 1976. Surface waves in a vertically inhomogeneous halfspace with a weak lateral inhomogeneity. *Izv. AN SSSR, Fiz. Zem.* **4,** 24–31.

Bache, T.C., 1982. Estimating the yield of underground nuclear explosions, *Bull. seism. Soc. Am.*, **72,** S131–S168.

Bache, T.C., Day, S.M. & Swanger, H.J., 1982. Rayleigh wave synthetic seismograms from multidimensional simulations of underground explosions, *Bull. seism. Soc. Am.*, **72,** 15–28.

Bache, T.C., Rodi, W.L. & Harkrider, D.G., 1978. Crustal structures inferred from Rayleigh-wave signatures of NTS explosions, *Bull. seism. Soc. Am.*, **68,** 1399–1413.

Båth, M., 1967. Recommendations of the IASPEI committee on magnitudes, *Seism. Bull.*, May volume, Seismological Institute, Uppsala.

Basham, P.W., 1969. Canadian magnitudes of earthquakes and nuclear explosions in south-western North America, *Geophys. J. R. astr. Soc.*, **17,** 1–13.

Basham, P.W., 1971. A new magnitude formula for short period continental Rayleigh waves, *Geophys. J. R. astr. Soc.*, **23,** 255–260.

Basham, P.W. & Horner, R.B., 1973. Seismic magnitudes of underground nuclear explosions, *Bull. siesm. Soc. Am.*, **63,** 105–131.

Burridge, R. & Weinberg, H., 1977. Horizontal rays and vertical modes, *Wave Propagation and underwater acoustics*, Springer-Verlag, New York.

Day, S.M. & McLaughlin, K.L., 1991. Seismic Source Representation for Spall, *Bull. seism. Soc. Am.*, **81,** 191–201.

Evernden, J.F., 1971. Variation of Rayleigh-wave amplitude with distance, *Bull. seism. Soc. Am.*, **67,** 405–411.

Evernden, J.F. & Filson, J., 1971. Regional dependence of surface-waves versus body-wave magnitudes, *J. geophys. Res.*, **76,** 3303–3308.

Given, J.W. & Mellman, G.R., 1986. Estimating explosion and tectonic release source parameters of underground nuclear explosions from Rayleigh and Love wave observations, *Sierra Geophysics Inc. Rept. No. SGI-R-86-126,* AFGL-TR-86-0171, Kirkland, WA.

Glover, P. & Harkrider, D.G., 1986. Numerical tests of surface wave path corrections, *Science Applications International Corp. Rept. No. C86-05,* MDA903-84-C-0020, McLean, VA.

Gupta, I.N., Lynnes, C.S., Chan, W.W. & Wagner, R.A., 1989. A comparison of the spectral characteristics of nuclear explosions detonated below and above the water table, *Teledyne Geotech Rept. No, TGAL-89-04,* GL-TR-89-0151, Alexandria, VA.

Harkrider, D.G., 1981. Coupling near source phenomena into surface wave generation, *Identification of Seismic Sources—Earthquake or Underground Explosion,* pp. 277–326, eds Husebye & Mykkeltveit, D. Reidel, Dordrecht.

Harkrider, D.G. & Anderson, D.L., 1966. Surface wave energy from point sources in plane layered earth models, *J. geophys. Res.*, **71,** 2967–2980.

Lapin, L.L., 1983. *Probability and Statistics for Modern Engineering,* Brooks/Cole, Monterey, CA.

Larson, D.B., 1981. Explosive energy coupling in geologic materials, *Lawrence Livermore National Laboratory, Report UCID-85662.*

Levshin, A.L., 1985. Effects of lateral inhomogeneities on surface wave amplitude measurements, *Annales Geophysicae,* **3,** 511–518.

Lilwall, R.C. & Neary, J.M., 1985. Redetermination of earthquake body-wave magnitudes using ISC Bulletin data, United Kingdom Atomic Energy Authority, *AWRE Rept. No. O 21/85,* H.M.S.O., London.

Marshall, P.D. & Basham, P.W., 1972. Discrimination between earthquakes and underground explosions employing an improved M_S scale, *Geophys. J. R. astr. Soc.*, **28,** 431–458.

Marshall, P.D., Douglas, A. & Hudson, J.A., 1971. Surface waves from underground nuclear explosions, *Nature,* **234,** 8–9.

Marshall, P.D., Lilwall, R.C. & Farthing, J., 1986. Body wave magnitudes and locations of underground nuclear explosions at Nevada Test Site 1971-1980, United Kingdom Atomic Energy Authority, *AWRE Rept. No O 21/86,* H.M.S.O., London.

Marshall, P.D., Springer, D.L. & Rodean, H.C., 1979. Magnitude corrections for attenuation in the upper mantle, *Geophys. J. R. astr. Soc.*, **57,** 609–638.

Mueller, R.A. & Murphy, J.R., 1971. Seismic characteristics of underground nuclear detonations, *Bull. seism. Soc. Am.*, **61,** 1675–1692.

Murphy, J.R., 1977. Seismic source functions and magnitude determinations for underground nuclear detonations, *Bull. seism. Soc. Am.*, **67,** 135–158.

Patton, H.J., 1988. Application of Nuttli's method to estimate yield of Nevada Test Site explosions recorded on Lawrence Livermore National Laboratory's Digital Seismic Systems, *Bull. seism. Soc. Am.*, **78,** 1759–1772.

Patton, H.J., 1991. Seismic moment estimation and the scaling of the explosion source, *Geophysical Monograph 65: Explosion Source Phenomenology,* pp. 171–183, eds Taylor, S.R., Patton, H.J. & Richards, P.G., *Am. geophys. Un. Monogr.,* Washington, DC.

Saito, M., 1967. Excitation of free oscillations and surface waves by joint sources in a vertically heterogeneous earth. *J. geophys. Res.*, **72,** 3689-3699.

Schlittenhardt, J., 1988. Seismic Yield Estimation Using Teleseismic *P*- and *PKP*-waves Recorded at the GRF-(Graefenberg) array, *Geophys. J.*, **95,** 163–179.

Springer, D.L., 1966. *P*-wave coupling of underground explosions, *Bull. seism. Soc. Am.*, **56,** 861–876.

Stevens, J.L., 1986. Estimation of scalar moments from explosion-generated surface waves, *Bull. seism. Soc. Am.*, **76,** 123–151.

Stevens, J.L., 1991. Seismic source characteristics of cavity decoupled explosions in salt and tuff, *Bull. seism. Soc. Am.*, **81,** 1272–1291.

Springer, D.L. & Kinnaman, R.L., 1971. Seismic source summary for U.S. underground nuclear explosions, 1961–1970, *Bull. seism. Soc. Am.*, **61,** 1073–1098.

Stevens, J.L. & McLaughlin, K.L., 1988. Analysis of surface waves from the Novaya Zemlya, Mururoa, and Amchitka Test Sites, and maximum likelihood estimation of scalar moments from earthquakes, *S-CUBED Technical Rept. No. SSS-TR-89-9953,* F08606-85-c-0028, La Jolla, CA.

Sykes, L.R. & Cifuentes, I.L., 1984. Yields of Soviet underground nuclear explosions from seismic surface waves: compliance with the Threshold Test Ban Treaty, *Proc. Natl Acad. Sci. U.S.A.*, 1922–1925.

Taylor, S.R., 1983. Three-dimensional crust and upper mantle structure at the Nevada Test Site, *J. geophys. Res.*, **88,** 2220–2232.

Taylor, S.R. & Randall, G.E., 1989. The effects of spall on regional seismograms, *Geophys. Res. Lett.*, **16,** 211–221.

Vergino, E.S. & Mensing, R.W., 1989. Yield estimation using regional mb(Pn), *Lawrence Livermore National Laboratory Report UCID-101600.*

von Seggern, D., 1973. Joint magnitude determination and analysis of variance for explosion magnitude estimates, *Bull. seism. Soc. Am.*, **63,** 827–845.

von Seggern, D., 1977. Amplitude distance relation for 20-Second Rayleigh waves, *Bull. seism. Soc. Am.*, **67,** 405–511.

Werth, G.C. & Herbst, R.F., 1963. Comparison of amplitudes of seismic waves from nuclear explosions in four mediums, *J. geophys. Res.*, **68,** 1463–1475.

Woodhouse, J.H., 1974. Surface waves in a laterally varying layered structure, *Geophys. J. R. astr. Soc.*, **37,** 461–490.

Yacoub, N.K., 1983. Instantaneous amplitudes: a new method to measure seismic magnitude, *Bull. seism. Soc. Am.*, **73,** 1345–1355.

Yanovskaya, T.B., 1989. 2. Surface waves in media with weak lateral inhomogeneity, in *Seismic Surface Waves in a Laterally Inhomogeneous Earth,* ed. Keilis-Borok, V.I., Kluwer Academic Publishers, Dordrecht.

Yomogida, K., 1985. Surface waves in a laterally slowly-varying media, *Geophys. J. R. astr. Soc.*, **82,** 511–533.

Zhao, L.S. & Harkrider, D.G., 1992. Wavefields from an off-center explosion in an imbedded solid sphere, *Bull. seism. Soc. Am.*, **82,** 1927–1955.